

Doctoral thesis

Long range dependence in discharge time series and its relationship to external drivers

submitted in satisfaction of the requirements for the degree of
"Doktor der technischen Wissenschaften", "Dr.techn."

as part of the
Vienna Doctoral Programme on Water Resource Systems

by

Dipl.-Math. Elena Szolgayová
Mudroňova 28
81101 Bratislava, Slovakia

Examiners:

Univ.Prof. Dipl.-Ing. Dr.techn. Christian Bucher
Institute of Building Construction and Technology
Vienna University of Technology

Univ.Prof. Dipl.-Ing. Dr.techn. Günter Blöschl
Institute of Hydraulic Engineering and Water Resources Management
Vienna University of Technology

Prof. Alberto Montanari
Department DICAM, Faculty of Engineering
University of Bologna

September 30, 2014

Abstract

The long term analysis of hydrological variables, such as discharge, is important given the recent interest in climate change effects on the water balance of catchments. The aim of this thesis is to gain deeper understanding of the long term behaviour of discharge and its possible dependencies on various climate and storage related drivers from a long term perspective. There are several criteria that can be considered, when analysing time series from a long term perspective. Long range dependence, measured by the Hurst coefficient, gives information about the autocorrelation for high time lags. This phenomenon is investigated in Chapter 3, where the Hurst coefficient of 39 series of mean daily discharges of European rivers is estimated using different methods. The existence of long range dependence is identified in all time series. Furthermore, the correlations between the Hurst coefficient and several discharge related characteristics are investigated. Various significant correlations are found including a positive correlation between the Hurst coefficient and catchment area and air temperature. Another approach of analysing hydrological variables from a long term perspective are wavelet and cross-wavelet spectra. This methodology is used in Chapter 4 to analyse monthly time series from the Danube River in order to find long cycles. The correlations between the spectra are examined for discharge, air temperature and precipitation monthly data sets. Long cycles with over a decade long return periods are found in all discharge time series. Long cycles in selected precipitation time series are found as well. However, no long cycles can be identified in the air temperature time series. The cross-wavelet analysis shows strong correlations between the discharge and precipitation spectra, especially for low frequencies. The two approaches mentioned above are combined in Chapter 5, where a method for deseasonalisation of time series using discrete wavelet transformation is proposed. Long range dependence of the time series is taken into consideration by using an ARFIMA (autoregressive fractionally integrated moving average) model. Wavelet deseasonalisation is compared to a standard moving average deseasonalisation approach, using forecasting performance as a comparison criterion. The results show that, considering one to ten days ahead forecasting performance, the wavelet deseasonalisation approach improves the forecasting performance for longer forecasting horizons compared to the standard approach. The findings of this thesis give new insights into discharge and discharge related processes from the long term perspective. They form a basis for more accurate multivariate modelling, using discharge as dependent and possibly air temperature and precipitation as explanatory variables. The results of this thesis suggest that there are significant cycles with multidecadal time periods in European rivers. Furthermore, the results highlight the need to approach time series modelling on a case-by-case base, considering the specific periodic behaviour of each data set separately, emphasizing the need for future improvements of stochastic modelling of discharge processes.

Kurzfassung

Langzeitabhängigkeit von Abflusszeitreihen und die Rolle externer Einflussfaktoren

Langfristige Analysen hydrologischer Variablen wie der Abfluss sind in Hinblick auf die aktuelle Debatte rund um den Klimawandel und dessen Einfluss auf den Wasserkreislauf von großer Bedeutung. Das Ziel der vorliegenden Arbeit ist es, ein besseres Verständnis des Langzeitverhaltens des Abflusses und dessen Abhängigkeiten von verschiedenen klimabezogenen und speicherbezogenen Einflussfaktoren zu erlangen. Zeitreihen können mittels verschiedener Methoden aus einer Langzeitperspektive untersucht werden. Die Langzeitpersistenz, die anhand des Hurst-Koeffizienten quantifiziert wird, gibt Auskunft über die Autokorrelation auf großen Zeitskalen. Dieses Phänomen wurde in dieser Dissertation zunächst im Kapitel 3 untersucht. Hierzu wurde der Hurst-Koeffizient für 39 europäische Zeitreihen von Tageswerten des Abflusses unter Verwendung fünf verschiedener Schätzmethode berechnet. Eine Langzeitpersistenz konnte in allen Zeitreihen nachgewiesen werden. Darüber hinaus wurde die Korrelation zwischen dem Hurst-Koeffizienten und mehreren abflussbezogenen Parametern untersucht. Einige signifikante Korrelationen wie zum Beispiel eine positive Korrelation zwischen dem Hurst-Koeffizienten und der Größe des Einzugsgebietes, beziehungsweise der Lufttemperatur konnten nachgewiesen werden. Eine Möglichkeit zur Analyse der Prozesse aus einer Langzeitperspektive ist die Bestimmung der Wavelet- und Crosswaveletspektren. Diese Methode wurde im Kapitel 4 angewandt um lange Zyklen in den monatliche Zeitreihen des Donauabflusses zu identifizieren. Korrelationen zwischen den Spektren des Abflusses, der Lufttemperatur und des Niederschlages wurden nachgewiesen. Lange Zyklen mit Zeitskalen von Dekaden konnten in allen Abflusszeitreihen identifiziert werden. Für manche Niederschlagszeitreihen wurden ebenfalls lange Zyklen gefunden, jedoch nicht für die Zeitreihen der Lufttemperatur. Die Crosswaveletanalyse zeigte insbesondere im Niederfrequenzbereich (lange Zeitskalen) eine signifikante Korrelation zwischen den Abfluss- und Niederschlagsspektren. Die beiden in den vorhergehenden Kapiteln verwendeten Methoden wurden in Kapitel 5 schließlich miteinander kombiniert. Hierbei wurde zusätzlich eine Methode eingeführt, die die diskrete Wavelettransformation mit Saisonalitätsbereinigung von Zeitreihen ermöglicht. Die Langzeitabhängigkeit der Zeitreihen wurde durch Anwendung eines ARFIMA (autoregressive fractionally integrated moving average) Modells berücksichtigt. Die Wavelet-Saisonalitätsbereinigung wurde sodann unter dem Gesichtspunkt der Vorhersageeffizienz mit einem gängigen Saisonalitätsbereinigungsansatz verglichen. Für eine Vorhersagefrist von 1 bis 10 Tagen zeigen die Ergebnisse, dass die Saisonalitätsbereinigung mittels des Wavelet-Modells die Vorhersageeffizienz verbessert,

besonders für die längeren Vorhersagefristen. Die Ergebnisse der hier vorliegenden Dissertation erlauben neue Einblicke in die Abfluss- und abflussbezogenen Prozesse aus einer Langzeitperspektive. Sie bilden somit die Grundlage für zukünftige multivariate Modelle, indem sie den Abfluss als abhängige Größe sowie die Lufttemperatur und den Niederschlag als erklärende Variablen ausweisen. Die Ergebnisse dieser Arbeit zeigen weiterhin, dass in europäischen Flüssen signifikante Zyklen mit Zeitskalen von mehreren Dekaden vorherrschen. Die hier vorgelegte Arbeit zeigt auf, dass die Zeitreihenmodellierung des Abflusses unter Anbetracht des jeweiligen spezifischen periodischen Verhaltens jedes einzelnen Datensatzes fallbezogen durchzuführen ist. Zukünftige Optimierungsansätze für die stochastische Modellierung abflussbezogener Prozesse müssen die langfristigen Abhängigkeiten berücksichtigen.

Acknowledgement

I would like to express my gratitude to my supervisors - Prof. Bucher and Prof. Blöschl, for their patience and professional expertise. I appreciate their dedication to the Water Resources doctoral programme and I could never have finished the PhD without their support and help.

Furthermore I would like to thank Prof. Arlt from the University of Economics in Prague for giving me the opportunity to do my research semester abroad at his institute and for his kind support. I would like to thank Milan Bašta for his time and patience, when I was utterly lost in wavelet modelling.

I would like to thank to the external reviewer of this thesis – Prof. Montanari, who took his time to discuss the long range dependence topic with me during a conference couple of years ago, giving me valuable inputs for my first publication.

I would like to thank my fellow students, especially Alicja Sobantka, who was an invaluable friend on this long journey. Last but not least I would like to thank my family - especially to my father for his advice and support and to my mother for giving me courage in my moments of desperation. I would like to thank to my sister, who always had my back, supporting me with stories from her own PhD, making me believe, I can do it as well.

Financial support for this work was provided by the Austrian Science Funds FWF (Doctoral Programme on Water Resource Systems, DK-plus W1219-N22) and the grants APVV-0073-10 and P402/12/G097 (topic covered in chapter 5).

Contents

List of Figures	x
List of Tables	xii
1 Introduction	1
2 Methods	5
2.1 Long range dependence and Hurst coefficient estimation	5
2.1.1 Long range dependence	5
2.1.2 Hurst coefficient estimation	5
2.2 Wavelet analysis	9
2.2.1 Continuous wavelet transform	9
2.2.2 Discrete wavelet transform	10
2.3 Deseasonalization	10
2.4 Time series models	11
2.4.1 ARFIMA	11
3 Factors influencing long range dependence in streamflow of European rivers	13
3.1 Introduction	13
3.2 Methodology	16
3.2.1 Correlation of Hurst coefficient and catchment attributes	16
3.3 Data description	17
3.4 Results	19
3.4.1 Estimation of the Hurst coefficient	19
3.4.2 Correlation between Hurst coefficient and catchment attributes	23
3.5 Discussion and conclusions	27
4 Long term variability of the Danube River flow and its relation to precipitation and air temperature	33
4.1 Introduction	33
4.2 Data and methods	35
4.2.1 Discharge convolution	37
4.3 Results	38
4.3.1 Long cycles	38
4.3.2 The cross - wavelet spectra and wavelet coherence	39
4.3.3 Convoluted data	41

4.4	Discussion and conclusions	45
5	Wavelet based deseasonalization for modelling and forecasting of daily discharge series considering long range dependence	49
5.1	Introduction	49
5.2	Methods	51
5.2.1	Description of the models	52
5.2.2	Forecasts comparison	53
5.3	Results	54
5.3.1	Model fit	54
5.3.2	Forecasting comparison	58
5.4	Discussion and conclusions	59
6	Summary of results and conclusions	63
	Appendix A	75
	Appendix B	77

List of Figures

3.1	Location of the stream gauges in Europe	18
3.2	Estimated Hurst coefficients of daily runoff H for all methods. On the horizontal axes are the indices of the runoff time series, ranked in ascending order of H of the periodogram regression method.	20
3.3	Estimated Hurst coefficients of daily runoff for all estimation methods.	21
3.4	Scatter plots of the Hurst coefficients of daily runoff estimated by different estimation methods. Range of the axes is from 0.5 to 1 in all cases.	22
3.5	Dependency of the Hurst coefficient of daily runoff (estimated using the regression on periodogram) on catchment area, mean annual air temperature, mean annual precipitation, elevation, mean discharge, specific mean discharge, seasonality of runoff (maximum Pardé coefficient) and the length of the runoff time series. The green line represents a moving average over 5 data points.	24
3.6	Dependency of the Hurst coefficient of daily runoff (estimated using the Whittle method) on catchment area, mean annual air temperature, mean annual precipitation, elevation, mean discharge, specific mean discharge, seasonality of runoff (maximum Pardé coefficient) and the length of the runoff time series. Bars indicate 95% confidence intervals of H . The green line depicts a moving average over 5 data points.	25
3.7	Hurst coefficients of daily runoff for the stations at the Danube River. Stations are ordered according to their position on the river, Regensburg being the closest to the spring of the Danube and Orsova the most downstream of the stations analyzed.	30
4.1	Geographical position of discharge, precipitation and climatological gauges including the catchment area boundaries.	36
4.2	The global wavelet spectra of the discharge, precipitation and temperature time series. The dotted line represents the 95 percent confidence bound.	39
4.3	Example of the global wavelet spectra of mean monthly precipitation time series used for the calculation of the catchment average precipitation series. The dotted lines indicate the 95 percent confidence bounds of a red noise global wavelet spectrum.	40
4.4	Daily minimum temperatures for each year for the Kienstock catchment average temperature time series. The red line indicates the time period, where the wavelet spectrum is significant in power for the low frequencies (over 5 years periodicity).	41

4.5	The wavelet spectra for each of the analysed variables - discharge, catchment average precipitation and air temperature.	42
4.6	The cross - wavelet and wavelet coherence spectra. The first two rows show the cross - wavelet spectra between precipitation/discharge and air temperature/discharge respectively. The bottom two rows show the wavelet coherence spectra for the same pairs of variables. Arrows show the phase shift between the respective time series. Colours indicate the measure of coherence - red colour implies high degree of coherence. Arrows pointing right indicate that the two time series are in phase. Arrows pointing down indicate that precipitation/temperature leads discharge.	43
4.7	The wavelet (left), cross - wavelet (middle) and coherence spectra (right) for the discharge time series calculated from the Bratislava precipitation time series using the kernel combining 10 days and 5 years travel times with respective weights 0.1 and 0.9.	45
5.1	Analysis overview	51
5.2	Danube daily discharge at the Kienstock gauge, period 1.1.1992 - 31.12.2006 (left) and the periodogram of the time series (right)	55
5.3	The image on the top shows the series used for deseasonalization; the moving average of daily means and the wavelet filter, both for the period 1992-2006. The bottom image is the wavelet spectrum of the time series for the corresponding period. The white band in the lower part of the figure corresponds to the annual periodicity, as indicated on the vertical axis of the figure.	56
5.4	Autocorrelation function of the time series. The left pictures show the (logarithm) of the original runoff time series and its autocorrelation function. The figures on the right depict the autocorrelation function after deseasonalization (using wavelets in the middle and using the moving average subtraction on the right) and the respective residual series. In the bottom of the Figure there are the periodograms calculated after the application of the respective deseasonalization method.	57
5.5	The smooth and detail time series components calculated using the (inverse) Haar wavelet transform (model 3)	58
5.6	Autocorrelation function of the residuals for each of the three applied models. The dashed lines depict the significance bounds.	59
5.7	Scatterplots of measured daily discharges versus the forecasted discharges using all three models. Forecasting horizons of 1, 3, 6 and 10 days are shown. 60	60

List of Tables

3.1	Number of stream gauges and streamflow record length by country . . .	18
3.2	Kendall's τ correlations between the Hurst coefficients of daily runoff estimated by different methods	20
3.3	Spearman's ρ correlations between the Hurst coefficients of daily runoff estimated by different methods	20
3.4	Deviations of the H estimates of daily runoff for each estimation method from the mean of all estimators in terms of root mean squared error. . .	23
3.5	Kendall's τ correlations between Hurst coefficients of daily runoff and catchment attributes. Those τ , where the independence hypothesis was rejected on a 95% level are printed in bold. Rightmost column shows the average τ over all estimation methods.	26
3.6	Spearman's ρ correlations between Hurst coefficients of daily runoff and catchment attributes. Those ρ , where the independence hypothesis was rejected on a 95% level are printed in bold. Rightmost column shows the average ρ over all estimation methods.	26
3.7	Kendall's τ correlations between the catchment attributes. Those τ , where the independence hypothesis was rejected on a 95% level are printed in bold. $\log(A_i)$ is the log of the catchment area, T_i and P_i are the mean annual temperature precipitation respectively, E_i is the mean catchment elevation, $\log(\bar{Q}_i)$ and q_i are the log mean and specific discharge, Pk_i is the seasonality expressed by the Pardé coefficient and N_i is the time series length in years.	28
3.8	Spearman's ρ correlations between the catchment attributes. Those ρ , where the independence hypothesis was rejected on a 95% level are printed in bold. $\log(A_i)$ is the log of the catchment area, T_i and P_i are the mean annual temperature precipitation respectively, E_i is the mean catchment elevation, $\log(\bar{Q}_i)$ and q_i are the log mean and specific discharge, Pk_i is the seasonality expressed by the Pardé coefficient and N_i is the time series length in years.	28
4.1	Data description for the four data sets sorted according to the discharge gauge. All four discharge gauges are on the Danube River. For all time series of monthly data the time interval November 1901 - October 2006 (105 years) was used. The descriptive statistics are given for non-desaseaonalized data. The Hurst coefficients were estimated using the regression on periodogram and the detrended fluctuation analysis (DFA).	37

4.2	Hurst coefficient estimates for daily convoluted discharge time series. The Hurst coefficients of the real precipitation and discharge time series are listed in the first two rows. Hurst coefficients for different weight combinations and different travel times are listed in the following rows. The Hurst coefficient was estimated using regression on periodogram (Per.Reg.) and detrended fluctuation analysis (DFA).	44
5.1	Parameters of the fitted ARFIMA models (equation 2.30)	58
5.2	Forecasting performance comparison - outputs from the Nash - Sutcliffe coefficient (E) and the Theil's coefficient (U) and the modified Diebold Mariano test (MDM). For the MDM test, the comparison model is given in parentheses.	61
A-1	Description of the runoff data used in this study, including the Hurst coefficient estimates from all five methods. N_i is the time series length (years), A_i is the catchment area (km^2) and P_i is the mean annual precipitation (mm).	75

Chapter 1

Introduction

In the last years, there has been a dramatic increase in the interest in climate related topics, including the impact of the changing climate on river flows. In order to address this issue, the study of long histories of discharge series is necessary. Furthermore, discharge has to be seen as a part of the system of climate and storage related variables, such as air temperature. This is a natural approach, when conceptual discharge modelling is concerned. However, stochastic time series models usually consider only a short history of the discharge, and other external variables often are not considered at all.

With the increase of general data availability and quality, the analysis of river flows from a long term perspective becomes possible and significantly easier than before. This allows including long term effects into time series models as well. In order to improve time series modelling, especially when multivariate models are considered, it is first necessary to observe and mathematically express dependencies between discharge and related drivers such as air temperature and precipitation. Such multivariate models will ultimately contribute to managing water resources in river basins in a more efficient way.

Analysing discharge and related variables is a quite complex issue, from both philosophical and mathematical perspectives. Even though long data records are often available, the actual amount of data is always limited. This may lead to wrong interpretations of the events occurring. For example, what may actually be a long cycle in the time series may be interpreted as a trend (Blöschl and Montanari, 2010), possibly leading to severe imperfection in the performance of hydrological models. In general, the importance of cycles has already been pointed out in Probst and Tardy (1987), who found that, on the European scale, the river flows "show progressive shifts or lags in the correspondence between dry and wet periods", meaning the fluctuations between dry and wet periods are "similar but shifted", for example for the Loire, Elbe and Ural Rivers. Even if the presence of a trend is acknowledged, failure to incorporate serial and cross correlations in trend analyses may result in erroneous conclusions (Khaliq et al., 2009). The situation becomes even more complex when the climatic drivers influencing the river flows are considered. Several authors attempted to explain these influences, sometimes on a global scale. Andreo et al. (2006) showed that, despite the increase of air temperatures on the Iberian peninsula in Spain, no long term trend in the distribution was detected. Other authors point out the importance of incorporating these forcings in general (Koutsoyianis, 2003, Probst and Tardy, 1989). Most of such studies however focus on the influence of global climatic phenomena such as the North Atlantic Oscillation (Massei et al., 2010,

Ouachani et al., 2013, Torrence and Webster, 1999). Studies analysing local drivers are more scarce.

Already in the 1950s, the British hydrologist H.E.Hurst observed that, in the flow of the Nile River where extremely long series of measurements were available, the data is correlated even for high temporal lags. This would mean that this year's floods or droughts would be correlated with events occurring for example 50 years ago. This effect will have a significant impact on the performance of discharge simulations, if present in the time series. Here several questions arise. Is this long term persistence observable in river flows in Europe, where the climatic conditions are varying over different regions and are generally different from those in Egypt? Is it possible to capture this effect when only shorter time series are available (which is the case, since the Nile time series contains over 600 years of data)? Do different estimation methods produce comparable results? And even more interestingly, how does long range dependence in discharge correlate with various climate and storage related drivers, such as catchment area, elevation, precipitation or air temperature?

The assumption that the events, processes and variables influencing the river flows are not statistically changing over time does not necessarily need to be correct, since the variables driving the discharge and thus the flood events, such as air temperature or precipitation, display changing behaviour due to general climatic variability. Other controls, such as diverse anthropogenic influences and developments vary over time as well. Thus a question arises whether there is a measurable dependence between river flow and these external climatic drivers, which is observable clearly enough and how this dependence can be mathematically expressed. Furthermore, it can be investigated whether it is possible to include these external drivers into stochastic models and thus obtain improvements in the model fit and simulations.

The aim of this thesis is to deepen the understanding of discharge and its driving processes from a long term perspective, thus creating a framework for improvements in stochastic time series modelling. Using various methods, the following questions will be explored: How are the climate or storage related drivers related to long term fluctuations of river discharges of European Rivers? Are there long cycles present in discharge, air temperature and precipitation time series on the Danube River? How can the detailed information about cyclical behavior of discharge series be used to improve forecasting performance of a statistical data driven discharge model?

The thesis is structured as follows:

Chapter 2 gives a detailed overview of the general theoretical background used in the rest of the thesis, including Hurst coefficient estimation, discrete and continuous wavelet analysis, deseasonalisation and the time series modelling procedure.

Chapter 3 focuses on the presence of long range dependence, measured by the Hurst coefficient, in annual discharge of European rivers. Several different methods are used for the Hurst coefficient estimation and the outputs are compared. Furthermore, an analysis of the correlations between the long range dependence with various external drivers, such as precipitation, temperature, catchment area and elevation is conducted.

Chapter 4 applies continuous wavelet analysis to examine long term cyclical behavior of monthly discharges of the Danube River. Furthermore, cross-wavelet analysis is applied to find dependencies between long cycles in discharge, precipitation and air temperature time series. Again, Hurst coefficients are calculated and compared to the cyclical behavior

observed in the wavelet spectra.

Finally, Chapter 5 deals with time series modelling under consideration of long range dependence. Here, the methods from the previous chapters are combined and a modification to an existing deseasonalisation procedure of time series is proposed, in order to improve the model forecasting performance of time series with long range dependence. The model is applied to a series of daily discharges from the Kienstock gauge on the Danube River and is evaluated based on its forecasting performance.

Chapter 6 summarises the findings of the thesis and gives a brief overview of possible future research.

Chapter 2

Methods

This chapter contains the mathematical background common to all the following chapters. Details considering the methodology will be furthermore discussed in each chapter separately to provide a more consistent image.

2.1 Long range dependence and Hurst coefficient estimation

2.1.1 Long range dependence

A time series $X_t, t = 1, \dots, T$ with long range dependence can be characterized by a hyperbolic decrease of the autocorrelation function $\rho_\tau = \text{Corr}[X_t, X_{t+\tau}]$

$$\rho_\tau \sim C\tau^{2H-2} \quad \tau \rightarrow \infty \quad (2.1)$$

where $\rho_\tau = \text{Corr}[X_t, X_{t+\tau}]$ is the autocorrelation function of a weakly stationary time series $X_t, t = 1, 2, \dots$ with finite variances (Montanari et al., 1999b) and C is a constant (note that stationarity does not exclude the possibility of long memory, because even for high lags, autocorrelation might still depend only on the time lag). Long range dependence is numerically expressed by the Hurst coefficient $H \in (0.5, 1]$. In general holds $H \in [0, 1]$. For $H = 0.5$ the time series is random noise. For $H < 0.5$ the time series is said to be antipersistent but this case is rarely of interest in hydrology (Koutsoyiannis, 2005).

2.1.2 Hurst coefficient estimation

There are numerous methods for estimating the Hurst coefficient Teverovsky et al. (1995). Details on estimation methods including a literature overview can be found in section 3.1. The methods used in this thesis are described in this section.

Rescaled range statistics

Assume observation time series of length N and let $Y(n) = \sum_{i=1}^n X_i$ be a series of partial sums of the runoff time series X_t .

Then the rescaled range $R/S(n)$ (Hurst, 1951) is defined as

$$R/S(n) = \frac{\max_{0 \leq t \leq n}(Y(t) - \frac{t}{n}Y(n)) - \min_{0 \leq t \leq n}(Y(t) - \frac{t}{n}Y(n))}{(\frac{1}{n} \sum_{i=1}^n X_i^2 - \frac{1}{n^2}Y(n)^2)^{1/2}} \quad (2.2)$$

In case of long memory

$$E(R/S(n)) \sim Cn^H \quad \text{as } n \rightarrow \infty \quad (2.3)$$

where C is a constant, n is the number of observations and H is the Hurst coefficient.

By taking the logarithm of equation 2.3 we obtain

$$\ln(E(\frac{R(n)}{S(n)})) = H \ln(n) + \ln(C) \quad (2.4)$$

Now let us consider a subdivision of the time series into K blocks of size N/K and let $k_i = iN/K$ be the starting points of each block. In order to obtain the estimator of H , equation 2.2 is first evaluated for each n and k_i as far as $k_i + n \leq N$, thus obtaining a series $R(k_i, n)/S(k_i, n)$ for each starting point k_i and for each length n . The Hurst coefficient estimate is then given by the slope of a regression line between $\ln(n)$ and the logarithm of the rescaled range $R(k_i, n)/S(k_i, n)$.

According to (Teverovsky et al., 1995), the "low end" of the plot is not suitable for estimation, since any possible short range dependence in the time series would result in a "transient zone" (as described in Salas et al. (1979)) in this area. The very high end of the plot is not suited either, since here too few points are present to make "reliable estimates". For this reason we estimated the Hurst coefficient only from the $R(k_i, n)/S(k_i, n)$ from the central part of the plot (Montanari et al., 1997).

Regression on the periodogram

Geweke and Porter-Hudak (1983) showed, that when considering the periodogram of the time series given by

$$I(\lambda) = \frac{1}{2\pi N} \left| \sum_{j=0}^{N-1} X_j e^{-ij\lambda} \right|^2 \quad \left\{ \omega = \frac{2\pi k}{N}; \forall k = 1, \dots, T \right\} \quad (2.5)$$

where $T = u_l \lfloor \frac{n-1}{2} \rfloor$, λ are the frequencies, the following equation holds:

$$\ln(I(\lambda)) \sim c - d \ln(4 \sin^2(\lambda/2)) \quad (2.6)$$

where c is a constant (dependent on the variance of the time series).

Thus fitting a regression line on the logarithm of the frequencies and logarithm of the periodogram delivers an estimate for d with $d = 1 - 2H$. T gives the upper limit for the frequencies used in the regression. As suggested in Taqqu and Teverovsky (1998) we use $u_l = 0.1$, i.e. the bottom 10% of the frequencies.

Whittle estimator

The Whittle estimator is a likelihood based method from the frequency domain. The Hurst coefficient is obtained by minimizing the function

$$Q(H) = \int_{-\pi}^{\pi} \frac{I(\lambda)}{f(\lambda, H)} d\lambda \quad (2.7)$$

where $I(\lambda)$ is defined as in Equation 2.5 and $f(\lambda, H)$ is the spectral density. While performing the actual minimization, equation 2.7 is discretized to (Beran, 1994)

$$Q(H) = \sum_{j=1}^{[(N-1)/2]} \frac{I(\lambda_j)}{f(\lambda_j, H)} \quad (2.8)$$

and it is assumed, that the data follows either a fractionally integrated moving average process $ARFIMA(p, d, q)$ or a fractional Gaussian noise (with $d = H - 0.5$). We assumed an $ARFIMA(p, d, q)$ process.

The parameters p, q were obtained by fitting a $ARFIMA(p, d, q)$ model to some of the runoff series for all combinations of the parameters based on the (partial) autocorrelation function. We then selected the most appropriate model based on the minimum of the Akaike criterion. Since the choice of $p = 1, q = 1$ was suitable for the series analyzed, we used these parameters for all time series in the study.

For the Whittle estimator construction of confidence intervals is possible. We constructed 95% confidence intervals as $(H - 1.96(V/N)^{0.5}, H + 1.96(V/N)^{0.5})$. Where $V = 2D^{-1}$ with $D_{ij} = 1/2\pi \int_{-\pi}^{\pi} \frac{\partial}{\partial \theta_i} \log f(\lambda) \frac{\partial}{\partial \theta_j} \log f(\lambda) d\lambda$, is the estimator of variance obtained from equation 2.8 (Rosse, 1996).

Aggregated Variance

Consider the averaged aggregated series

$$X_i^k = \frac{1}{k} \sum_{l=(i-1)k+1}^{ik} X_l \quad i = 1, 2, \dots, \lfloor N/k \rfloor \quad (2.9)$$

Then the variance of this series is estimated by

$$\widehat{Var} X^{(k)} = \frac{\sum_{i=1}^{\lfloor N/k \rfloor} (X_i^{(k)} - \bar{X})^2}{N/k} \quad (2.10)$$

One plots the logarithm of the variances (equation 2.10) of the aggregated series (equation 2.9) against the respective aggregation length k . The points so obtained should lie on a straight line with slope $2H - 2$ from which H was estimated by regression. Only the central region of the plot was considered in the regression, since the short range dependencies affect the low end of the plot and an insufficient number of blocks affects the high end of the plot (Teverovsky et al., 1995).

Least squares based on variance

Another method in the temporal domain is the LSV method (Tyrallis and Koutsoyiannis, 2011). LSV estimates H and the variance of the time series simultaneously, offering an unbiased estimator of both parameters, if the assumption of self-similarity and normal distribution of the data is fulfilled. The method is based on a unbiased estimator of the variance of \bar{X}_n for long range dependent time series derived in Beran (1994). Denote $\gamma_\tau = Cov[X_t, X_{t+\tau}]$ the autocovariance function of X_t . Then based on

$$E(S^2) = \frac{N-1-2\sum_{k=1}^{N-1}(1-k/N)\rho_k}{N-1}\gamma_0. \quad (2.11)$$

and on the property of the series $Z^{(k)}$

$$Var(Z^{(k)}) = k^{2H}\gamma_0 \quad (2.12)$$

one obtains a bias for the variance estimate on all scales (depending on H):

$$E(S^{2(k)}) = \frac{N/k - (N/k)^{2H-1}}{N/k - 1}\gamma_0^k \quad (2.13)$$

Where $Z^{(k)}$ is defined as

$$Z_i^{(k)} = kX_i^{(k)} \quad (2.14)$$

and $S^{2(k)}$

$$S^{2(k)} = \frac{\sum_{i=1}^{N/k} (Z_i^{(k)} - \bar{Z}_i^{(N)})^2}{N/k - 1} \quad (2.15)$$

By minimizing an error function

$$e^2(\sigma^2, H) = \sum_{k=1}^{[n/10]} \frac{(E(S^{2(k)}) - s^{2(k)})^2}{k^p} \quad (2.16)$$

(which is done numerically) one obtains the estimate for H . This method furthermore allows a graphical depiction of the standard deviation against all scales (a climacogram (Koutsoyiannis, 2010)), thus providing a way to visually verify the validity of the scaling law for each scale.

Detrended fluctuation analysis

The detrended fluctuation analysis (DFA) was introduced by (Peng et al., 1994). In this paper the DFA of first order was used. Here the series of partial sums $Y_t = \sum_{i=1}^t (X_i - \bar{X})$ is divided into non-overlapping boxes of length l (where \bar{X} is the mean of X_t). Then for each box a fluctuation function is calculated as

$$F(l) = \frac{1}{l} \sqrt{\sum_{i=1}^l (Y_i - ia - b)^2} \quad (2.17)$$

where $a, b \in \mathbb{R}$ are regression coefficients. This procedure is repeated for different values of l and a log - log plot of $F(l)$ against l is constructed. A generalized version of the Hurst coefficient is then obtained as the slope of the regression line. Here $H > 1$ indicates a non - stationary unbounded process (Peng et al., 1995).

2.2 Wavelet analysis

We are interested in the behaviour of the time series with emphasis on low frequency events. Wavelet transform provides information about the time series for different frequency intervals, making it thus a suitable tool. Furthermore, the wavelet transform does not make the assumption of stationarity of the analyzed time series.

2.2.1 Continuous wavelet transform

A continuous wavelet transform of a discrete signal (time series) $X_t, t = 0, \dots, T - 1$ with a constant time step δt is defined as

$$W_X(s, u) = \sum_{t=0}^{T-1} X_t \psi_{s,u}^*(t) \quad (2.18)$$

where

$$\psi_{s,u}(t) = \sqrt{\frac{\delta t}{s}} \psi\left(\frac{(t-u)\delta t}{s}\right) \quad (2.19)$$

is a family of functions obtained through translation and dilation of a mother wavelet $\psi_0(t) \in \mathbf{L}^2(\mathbb{R})$. $(*)$ denotes the complex conjugate, $s \in \mathbb{R} \setminus 0$ is the dilation (scale) parameter and $u \in \mathbb{R}$ is the translation parameter. A wavelet is an arbitrary function localized in time and frequency fulfilling the admissibility condition (Torrence and Compo, 1999, Vidakovic, 1999). The wavelet spectrum is calculated from the wavelet coefficients as $|W_X(s, u)|$. In this chapter 4 we use the Morlet wavelet $\psi(t) = \pi^{-1/4} e^{i\omega_0 t} e^{-t^2/2}$, where ω_0 denotes frequency. Even though there are many known wavelet functions (for some examples see e.g. Kaiser (1994)), the Morlet wavelet is very often chosen by practitioners for analysis of geophysical time series (Andreo et al., 2006, Grinsted et al., 2004, Labat, 2008, Lafreniere and Sharp, 2003).

Errors in the wavelet coefficients at the edges of the time series occur due to the finite length of the time series. These errors are taken into consideration by constructing a cone of influence (COI) of the wavelet spectrum. Within the COI such errors are negligible. The cone of influence is given by all points included in the support of the wavelet for each scale. For the Morlet wavelet it is the set of points (u, s) with $u \leq \sqrt{2}s$ (Mallat, 1998, Torrence and Compo, 1999).

Statistical significance of the wavelet spectrum is tested assuming the null hypothesis that the time series is randomly generated with autocorrelation properties of red noise. A five percent level of significance is used in the tests.

The global wavelet spectrum is defined as

$$\bar{W}_X^2(s) = \frac{1}{T} \sum_{i=0}^{T-1} |W_X(s, u)|^2 \quad (2.20)$$

Significant long cycles for each of the time series were tested comparing the global wavelet spectrum to the spectrum of a red noise process for each frequency interval. The red noise spectrum is approximated by an AR(1) process. The AR coefficient is calculated as $(\phi_1 + \phi_2^{0.5})/2$, where ϕ_1, ϕ_2 are the lag 1 and 2 correlations of the underlying time series. For details see (Grinsted et al., 2004, Torrence and Compo, 1999).

Cross - wavelet transform and wavelet coherence

Cross - wavelet transform and the wavelet coherence provide information about the relation between two time series. The cross - wavelet transform can be used as a measure of correlation between the wavelet spectra of two time series X_t, Y_t :

$$W_{X,Y}(s, u) = W_X(s, u)W_Y^*(s, u) \quad (2.21)$$

By normalizing the cross - wavelet transform the wavelet coherence is obtained

$$R_{X,Y} = \frac{|\langle s^{-1}W_{X,Y}(s, u) \rangle|^2}{\langle s^{-1}|W_{X,X}(s, u)|^2 \rangle \langle s^{-1}|W_{Y,Y}(s, u)|^2 \rangle} \quad (2.22)$$

where $\langle \cdot \rangle$ is a suitable smoothing operator (Torrence and Webster, 1999). In general $R_{X,Y}(s, u) \in [0, 1]$ holds. The significance tests for wavelet coherence and the cross - wavelet spectra are based on Monte Carlo simulations, for details see (Maraun and Kurths, 2004). Here the null hypothesis of no coherence between the two time series is made.

2.2.2 Discrete wavelet transform

Using multiresolution wavelet analysis, a signal can be approximated by

$$X_t \approx \sum_k s_{J,k} \phi_{J,k}(t) + \sum_{j=1}^J \sum_k d_{j,k} \psi_{j,k}(t) \quad (2.23)$$

where $\psi_{j,k} = 2^{-j/2} \psi(2^{-j}t - k)$ are functions obtained by translations and dilations of a mother wavelet $\psi(t)$, $\phi_{J,k} = 2^{-J/2} \phi(2^{-J}t - k)$ is obtained analogically from a father wavelet $\phi(t)$, $s_{j,k}, d_{j,k}$ are the wavelet transform coefficients and J is an integer. In general it holds $\int_{\mathbb{R}} \psi(t) dt = 0$ and $\int_{\mathbb{R}} \phi(t) dt = 1$. Furthermore the family of functions $\psi(2^{-j}t - k), j, k \in \mathbb{Z}$ form a basis of the $L^2(\mathbb{R})$ space. The parameters j, k localize the wavelet in frequency and time. For further properties of the wavelet functions see e.g. Starck et al. (1998). Equation (2.23) can be shortly rewritten as

$$X_t \approx S_{J,t} + \sum_{j=1}^J D_{j,t} \quad (2.24)$$

with $S_{J,t} = \sum_k s_{J,k} \phi_{J,k}(t)$ being the smooth signal and $D_{j,t} = \sum_k d_{j,k} \psi_{j,k}(t)$ being the detail signals for the frequency interval $(2^{-j-1}, 2^{-j})$.

For more details on the properties of the wavelet transform see e.g. Mallat (1998), Shensa (1992), Starck et al. (1998). There are several methods in the literature dealing with the implementation of discrete wavelet transform Gencay et al. (2001), Shensa (1992), Starck et al. (1998).

2.3 Deseasonalization

A strong annual seasonality is usually present in most of the geophysical time series. Chapter 5 elaborates on removing of the seasonality in detail. However, in all the following chapters the seasonality will be removed from the data prior to the analysis.

In order to remove seasonality in mean (as in chapters 3,5), a moving average of daily means is subtracted from the time series. Considering a time series with daily time step $X_t, t = 1, \dots, T$, than the 15 days two - sided moving average is calculated as

$$F_t = 1/15 \sum_{i=-7}^7 \bar{X}_{t+i} \quad (2.25)$$

with the series of averages calculated for each day of the year (and periodically extended accordingly)

$$\bar{X}_t = \frac{1}{n_y} \sum_{i=0}^{n_y-1} X_{(t \bmod 365)+365i} \quad (2.26)$$

where $n_y = \lceil T/365 \rceil$ is the number of years and leaving out the February 29th data. For F_t with $t \leq 7$ and $t \geq T - 7$ appropriate adjustments were made. Optionally, the moving average smoothing can be omitted from the deseasonalization process. The deseasonalized time series X_t^d is then obtained as

$$X_t^d = X_t - F_t \quad (2.27)$$

The seasonal effects in mean and variance (as in chapter 4) are removed by subtracting a series of monthly averages and dividing by the daily or monthly estimated standard deviations respectively as follows (Montanari et al., 2000) (considering monthly time step):

$$X_t^{des} = \frac{X_t - \bar{X}_t}{\sqrt{s_t^2}} \quad (2.28)$$

with the periodically extended series of monthly averages and estimated variances

$$\bar{X}_t = \frac{1}{n_y} \sum_{i=0}^{n_y-1} X_{(t \bmod 12)+12i} \quad \text{and} \quad s_t^2 = \frac{1}{n_y - 1} \sum_{i=0}^{n_y-1} (X_{(t \bmod 12)+12i} - \bar{X}_t)^2 \quad (2.29)$$

Here $n_y = \lceil T/12 \rceil$ is the number of years.

2.4 Time series models

2.4.1 ARFIMA

In order to capture long range dependence in the modelling process, an autoregressive fractionally integrated moving average model $ARFIMA(p, d, q)$ may be used:

$$(1 - \sum_{i=1}^p \phi_i B^i)(1 - B)^d X_t = (1 + \sum_{j=1}^q \theta_j B^j) \epsilon_t + c \quad (2.30)$$

where B is the backshift operator, ϕ_i and θ_j are the parameters of the autoregressive and moving average components of the model, c is a constant and d is the fractional parameter $d \in \mathbb{R}$ and $H = d + 0.5$. Thus in case of long term persistent processes holds $d \in (0, 0.5)$.

Chapter 3

Factors influencing long range dependence in streamflow of European rivers

Abstract

Investigating long range dependence of river flows, especially in connection with various climate and storage related factors, is important in order to improve stochastic models for long range dependence and in order to understand deterministic and stochastic variability in long term behaviour of streamflow. Long range dependence expressed by the Hurst coefficient H is estimated for 39 (deseasonalized) mean daily runoff time series in Europe of at least 60 years using five estimators (rescaled range, regression on periodogram, Whittle, aggregated variances, and least squares based on variance). All methods yield estimates of $H > 0.5$ for all data sets. The results from the different estimators are significantly positively correlated for all pairs of methods indicating consistency of the methods used. Correlations between H and various catchment attributes are also analysed. H is strongly positively correlated with catchment area. Apparently, increasing storage with catchment area translates into increasing long range dependence. H is also positively correlated with mean discharge and air temperature and negatively correlated with the mean specific discharge and the seasonality index (maximum Pardé coefficient). No significant correlation is found between the Hurst coefficient and the length of the analyzed time series. The correlations are interpreted in terms of snow processes and catchment wetness.

3.1 Introduction

The number of large scale studies analyzing long term behaviour of streamflows have increased dramatically in the past years. With better data availability and quality and with the rising interest of impact of climate change and climate related factors on streamflow processes (Blöschl and Montanari, 2010), the amount and complexity of these studies have increased. The importance of such research lies in the need of stochastic models incorporating long range dependence, which can be used for example in water resources

management or reservoir operations. It is also of interest to relate the long term behaviour to possible drivers causing these phenomena to understand the most important controls.

There are several ways of considering long term behaviour of streamflow, both from deterministic and stochastic perspectives. A common method is trend analysis. For example (Petrow et al., 2009) conducted a Germany - wide study of flood trends. They found increasing trends in several catchments and a strong dependence of the trends on atmospheric circulation patterns. (Stahl et al., 2010) found geographically coherent trend patterns of stream flow over Europe which they interpreted by climate drivers. For other large scale studies examining trends and their relation to external, especially climate related controls see (Kite, 1989, Kundzewicz et al., 2005, Schmocker-Fackel and Naef, 2010, Svensson et al., 2005).

Trends are only one phenomenon which is interesting from a long term perspective. (Kite, 1989) pointed out, that "what appears to be a trend now, may turn out to be part of a periodicity when looked at over a longer time span". Other long term dependencies of interest are therefore periodic events with frequencies as low as the data permit. (Gudmundsson et al., 2011), e.g., examined the response of low frequency components (in terms of relative variance) of runoff to the mean and long term variations of precipitation and air temperature. They suggest that the low frequency part of runoff follows atmospheric features but that the low frequency part of runoff is uncorrelated with the low frequency components of the climatic factors. However dependence on catchment properties and mean climatic conditions was found.

Another property characterizing time series from a long term perspective is the long range dependence (Hurst phenomenon (Hurst, 1951), Hurst - Kolmogorov dynamics or long term persistence). Here the autocorrelation function does not disappear even for high temporal lags (Grau-Carles, 2005), or "correlations decay like a power law" (Doukhan et al., 2003). Although this phenomenon has been known for over 60 years, it still remains largely unexplained and is hotly discussed in the literature. The point of contention is that, if random long range dependence is significant, some of the observed trends should not be interpreted in a causal way. For example (Koutsoyiannis et al., 2009) remark on the importance of "the understanding and modelling of the long-term variability of climatic processes ... with particular emphasis on the Hurst-Kolmogorov dynamics" and the need of communicating this across disciplines. (Koutsoyiannis and Montanari, 2007) point out that "the statistical uncertainty is dramatically increased in the presence of dependence, especially if this dependence is long term persistence" and highlight the need of examining this phenomenon with respect to "other climatic hypothesis". Alternatively, (Salas et al., 1979) considered the Hurst phenomenon as a pre - asymptotic feature, which can be reproduced by appropriate stationary models such as shifting mean models. Long range dependence can be numerically expressed by the Hurst coefficient H . This is a coefficient ranging between 0 and 1, where $H > 0.5$ indicates long range dependence in the data (see Section 2.1). There exists a wide range of methods for estimating the Hurst coefficient (an overview can be found for example in (Tevelevsky et al., 1995)), both in time and in the frequency domains. Historically, the first method used to estimate H is the rescaled range (R/S) analysis. This estimator does not account for short memory in the data nor for heteroscedasticity (Lo (1991)) and it suffers from "size distortions" for small data sets (Grau-Carles, 2005). Despite the numerous known drawbacks, the

rescaled range estimator is a rather popular method used in literature (Lye and Y.Lin (1994), Sakalauskiene (2003)). There are numerous papers examining estimators for artificially generated data with various properties. (Grau-Carles, 2005) compares estimators with respect to the length of the time series based on generated ARMA/GARCH series. He observes that the regression on periodogram method (developed by Geweke and Porter-Hudak (1983)) and the detrended fluctuation analysis outperform the other methods (R/S and modified R/S estimator), which often estimates $H > 0.5$ even if the time series was generated from a process without long range dependence. (Montanari et al., 1999b) generate series from a seasonal ARIMA model, to analyse the effects of periodic components on the H estimates. The Whittle estimator (Beran, 1994) turns out to be the most precise estimator despite the presence of short term dependencies. The Whittle estimator is a likelihood based method, which fits a fractionally integrated ARMA model to the data. The quality of the results depends on the correct choice of the underlying model, which might not be trivial. Furthermore the Whittle estimator assumes normal distribution of the time series, which is usually not the case considering hydrological data. Another method performing well in the tests of (Montanari et al., 1999b) is the aggregated variances algorithm. A comparison of twelve estimators applied to artificially generated series (using fractional Gaussian noise and fractionally integrated time series) was conducted by (Rea et al., 2009). They find the Whittle estimator to be among the most accurate methods when distinguishing time series with long memory and those with other non random components. (Tyralis and Koutsoyiannis, 2011) test twelve methods on generated fractional Gaussian noise series. In this study three methods estimating both the Hurst coefficient and the variance of the time series simultaneously are included. The authors conclude, that these three methods, a maximum likelihood estimator (McLeod and Hipel, 1978), least squares based on standard deviation (Koutsoyiannis, 2003) and a newly proposed method least squares based on variance (LSV) are "more accurate" compared to the other methods in test (including the rescaled range, regression on periodogram, the aggregated variances algorithm and a modification of the Whittle estimator - the local Whittle estimator (Robinson, 1995)). Furthermore, according to (Tyralis and Koutsoyiannis, 2011), the LSV method is computationally faster compared to the LSSD and ML algorithms, thus it is more suitable for long series of records, which is our case. The above listed studies analyze generated (artificial) time series with chosen properties where clear comparisons of estimated and prescribed Hurst coefficients can be established. However, a comparison can not be made based on real data, whose exact properties are never known.

There are several studies analyzing long range dependence on actual, non-artificial data using different methods. Local scale studies include (Montanari et al., 1999a, Radziejewski and Kundzewicz, 1997, Zhang et al., 2008), which all detect long range dependence in the discharge data sets.

On a larger scale, (Pelletier and Turcotte, 1997) conducted a study estimating the Hurst coefficient from average power spectra of monthly discharge data of 636 catchments in the United States and found long range dependence. (Koscielny-Bunde et al., 2006) conducted a study of 41 series of daily river runoff worldwide using wavelet based techniques, again having detected long range dependence in the data. (Ehsanzadeh and Adamowski, 2010) found long range dependence in weekly summer/winter low flows of approximately 200 Canadian stations and noted that long range dependence had strong influence on

trend estimation. (Lye and Y.Lin, 1994) tested long range dependence of peak flow series of 90 Canadian rivers based on rescaled range analysis and concluded there is "fairly high probability of long-term dependence". (Mudelsee, 2007) found H of monthly streamflow to increase along the stream network for four out of six rivers which they explained as a "result of spatial aggregation of short-memory reservoir contributions in the network". While there have been numerous studies testing for the presence of long range dependence in streamflow data, very little has been done on analysing the hydrological controls on the long range dependence. The aim of this chapter is therefore to analyze the long term behaviour of streamflow with respect to possible drivers. Specifically, we address the following questions: What are the Hurst coefficients of mean daily discharge time series of European rivers? Are the estimated Hurst coefficients consistent for various methods? What are the factors influencing the Hurst coefficient in these data? In order to address these questions, we first estimate the Hurst coefficients of discharge time series of European rivers using five different methods and examine the consistency of the results (meaning compare the Hurst coefficient estimates calculated by each of the methods). In a second step we correlate the Hurst coefficients so obtained with various catchment attributes to find possible drivers of long range dependence.

3.2 Methodology

Based on the literature (Grau-Carles, 2005, Koutsoyiannis, 2003, Montanari et al., 1999b, Tyrallis and Koutsoyiannis, 2011), five estimators of the Hurst coefficient were used in this chapter:

- Rescaled range (R/S),
- Regression on periodogram,
- Whittle estimator,
- Aggregated variances, and
- Least squares based on variance (LSV).

A description of the methods can be found in Chapter 2. The data were deseasonalized in mean prior to the Hurst coefficient estimation.

3.2.1 Correlation of Hurst coefficient and catchment attributes

As measures of correlation between the Hurst coefficient estimates and the catchment attributes Spearman's ρ and Kendall's τ are used. Spearman's ρ estimates, how well the dependence between the two considered variables can be expressed by a monotonic function. It is given by

$$\rho = \frac{\sum_{i=1}^{n_{TS}} (h_i - \bar{h})(a_i - \bar{a})}{(\sum_{i=1}^{n_{TS}} (h_i - \bar{h})^2 \sum_{i=1}^{n_{TS}} (a_i - \bar{a})^2)^{0.5}} \quad (3.1)$$

where h_i and a_i are the ranks assigned to the Hurst coefficient estimates and the catchment attributes, respectively. n_{TS} is the total number of the runoff time series analyzed.

Kendall's τ is based on rank comparison, assessing the number of same ordered pairs of each of the variables:

$$\tau = \frac{n_c - n_d}{0.5n_{TS}(n_{TS} - 1)} \quad (3.2)$$

where n_c and n_d are the number of concordant and discordant pairs, respectively. A pair of observations h_i, a_i is concordant if $h_i > a_i$ and discordant for $h_i < a_i$. Both of these correlation measures range between $(-1, 1)$. Values close to zero indicate in both cases that the variables are almost uncorrelated. The calculated values will be given with the result of a statistical test with the null hypothesis H_0 : The Hurst coefficient and the respective attribute are statistically uncorrelated.

3.3 Data description

Time series of mean daily discharges of European rivers were analyzed. The data were provided by the Global Runoff Data Center (GRDC, 2011) and by the UNESCO FRIEND database.

The character of the analyses requires as long records as possible, otherwise long and short term dependencies or trends can be difficult to distinguish (Montanari, 2003). In order to maintain relatively uniform spatial coverage of Europe and to minimize estimation uncertainty only data sets with a minimum length of 60 years were considered. The data were subject to preliminary analysis. The runoffs used in this chapter are originating mostly from large rivers, thus the effect of human interventions (such as urbanization or agriculture) on storage is expected to be small, with prevailing effects of the climate (Blöschl et al., 2007). However records with evident structural changes, such as shifts in the mean, which may have been due to anthropogenic influences such as dam or reservoir construction, were discarded. Records with missing data were not considered either. A total of 39 streamflow time series remained which are the basis of the analyses in this chapter. A brief overview of the dataset, including the number of records per country with the associated time series lengths is shown in Table 4.1. A more detailed overview including the estimation results, time series length and catchment areas is given in Table A-1. The geographical distribution of the stream gauges is shown in Figure 3.1.

The attributes, for which the correlations were estimated can be divided into two categories. The first group are the catchment characteristics, including climate:

- Log value of the catchment area $\log A_i$
- Mean annual air temperature T_i of the catchment area for the respective gauge for the period 1950 - 2000.
- Mean annual precipitation P_i of the catchment area for the respective gauge for the period 1950 - 2000.
- Mean elevation E_i of the catchment area

The second group contains runoff related characteristics including record length:

- Log value of the (longterm) mean of daily discharge $\log \bar{Q}_i$

Table 3.1: Number of stream gauges and streamflow record length by country

Country	Number of stations	Record lengths (years)
Austria	1	115 – 115
Czech Republic	2	88 – 92
Germany	10	82 – 159
Denmark	4	96 – 164
Finland	1	100 – 100
France	1	128 – 128
Italy	4	59 – 68
United Kingdom	2	126 – 135
Spain	3	63
Switzerland	2	96 – 98
Norway	6	87 – 127
Romania	1	150 – 150
Slovakia	2	94 – 107
Total	39	59 – 164

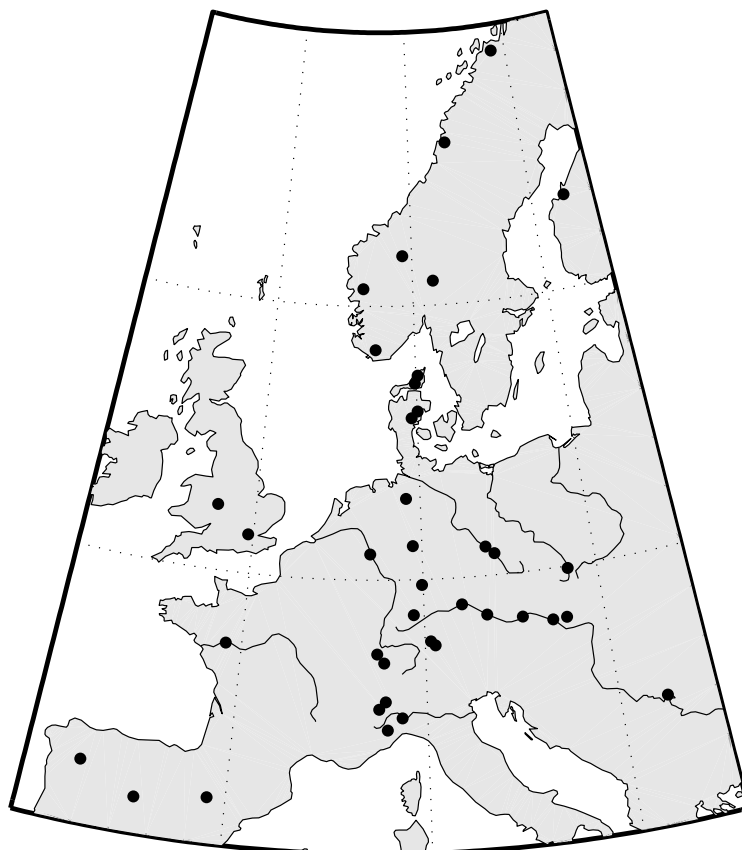


Figure 3.1: Location of the stream gauges in Europe

- Specific mean discharge $q_i = \bar{Q}_i/A_i$
- Seasonality of monthly flows expressed by the maximum Pardé coefficient (Pardé, 1947)

$$Pk_i = \max_{1 \leq j \leq 12} \left(\frac{12}{N_i} \sum_{l=1}^{N_i} \frac{Q_{jl}^{(i)}}{\sum_{j=1}^{12} Q_{jl}^{(i)}} \right) \quad (3.3)$$

where Q_{lj} is the mean monthly runoff for month j and year l . This value ranges between 1 and 12. Low values of Pk_i indicate rather uniform distribution of runoff over the year, whereas high values mean stronger presence of seasonal variations in runoff (Parajka et al., 2009).

- Log time series length (in days) N_i

Where $i = 1 \dots 39$ is the index of the station and N_i is the respective series length. The precipitation, elevation and temperature data were obtained from the Catchment Characterisation and Modelling database (Vogt et al., 2007).

3.4 Results

3.4.1 Estimation of the Hurst coefficient

The estimates for each method are shown in Figure 3.2. On the horizontal axes are the indices of the gauging stations ranked based on the periodogram regression estimation results. The estimated Hurst coefficients range between 0.57 and 1. This means that the analyses indeed suggest long range dependence for all data sets, using any of the methods. The aggregated variance method tends to give the lowest H estimates while the LSV method tends to give the largest H estimates. Indeed, according to the LSV method $H = 1$ for 21% of the rivers. Figure 3.3 shows the H estimates in a geographical context. According to all methods, except LSV, the Hurst coefficients are in general lower in Northern Europe (Norway and Finland) than in Central and Southern Europe. Another geographically consistent group are the four Italian catchments with Hurst coefficient lower than those in Central Europe for all but the aggregated variance method.

The agreement of the estimates is shown in more detail in Figure 3.4 as a scatter plot of pairs of estimators. In order to assess the degree of agreement of the estimators quantitatively, Kendall's τ and Spearman's ρ were calculated. The results are shown in Tables 3.2 and 3.3. All pairs of the estimators show significant positive correlations at the 95% significance level. The highest correlations are obtained between the R/S and aggregated variance estimators and the lowest correlations are obtained between LSV and aggregated variance estimators.

One way of comparing the estimators is calculating the root mean squared error of a respective estimator est

$$RMSE^{est} = \left(\frac{1}{n} \sum_{i=1}^n (H_i^{est} - \bar{H}_{all})^2 \right)^{1/2} \quad (3.4)$$

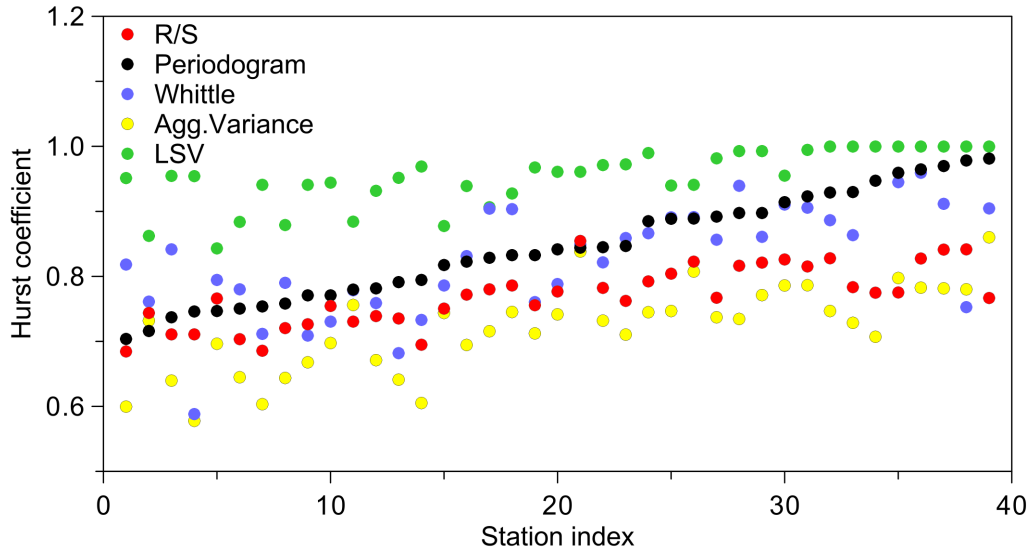


Figure 3.2: Estimated Hurst coefficients of daily runoff H for all methods. On the horizontal axes are the indices of the runoff time series, ranked in ascending order of H of the periodogram regression method.

Table 3.2: Kendall's τ correlations between the Hurst coefficients of daily runoff estimated by different methods

	R/S	Periodogram	Whittle	Agg. Variances	LSV	Average
R/S	1.00	0.62	0.49	0.67	0.36	0.53
Periodogram	0.62	1.00	0.47	0.56	0.65	0.58
Whittle	0.49	0.47	1.00	0.49	0.30	0.44
Agg. Variance	0.67	0.56	0.49	1.00	0.27	0.49
LSV	0.36	0.65	0.30	0.27	1.00	0.40

Table 3.3: Spearman's ρ correlations between the Hurst coefficients of daily runoff estimated by different methods

	R/S	Periodogram	Whittle	Agg. Variances	LSV	Average
R/S	1.00	0.80	0.67	0.84	0.52	0.70
Periodogram	0.80	1.00	0.64	0.76	0.81	0.75
Whittle	0.67	0.64	1.00	0.67	0.42	0.60
Agg. Variance	0.84	0.76	0.67	1.00	0.41	0.67
LSV	0.52	0.81	0.42	0.41	1.00	0.54

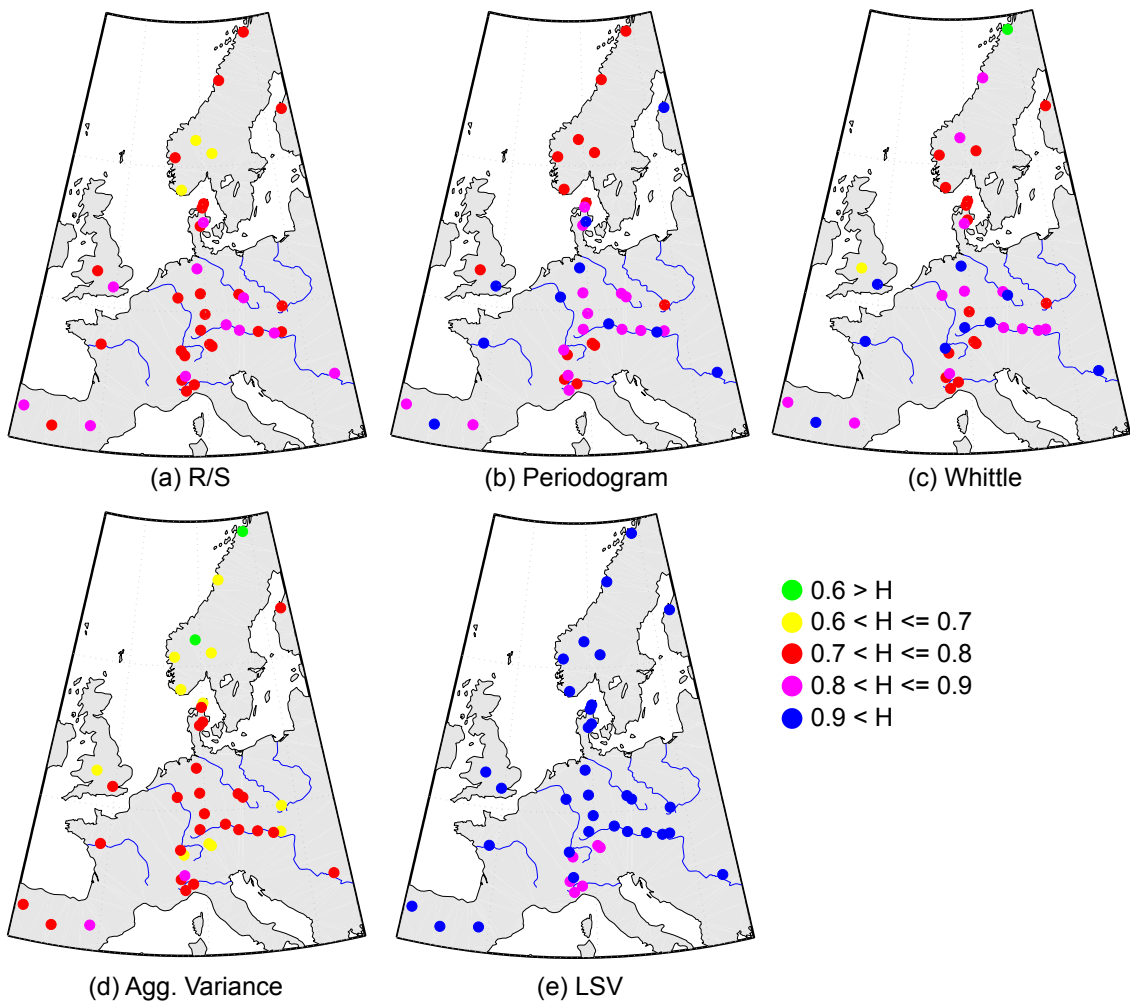


Figure 3.3: Estimated Hurst coefficients of daily runoff for all estimation methods.

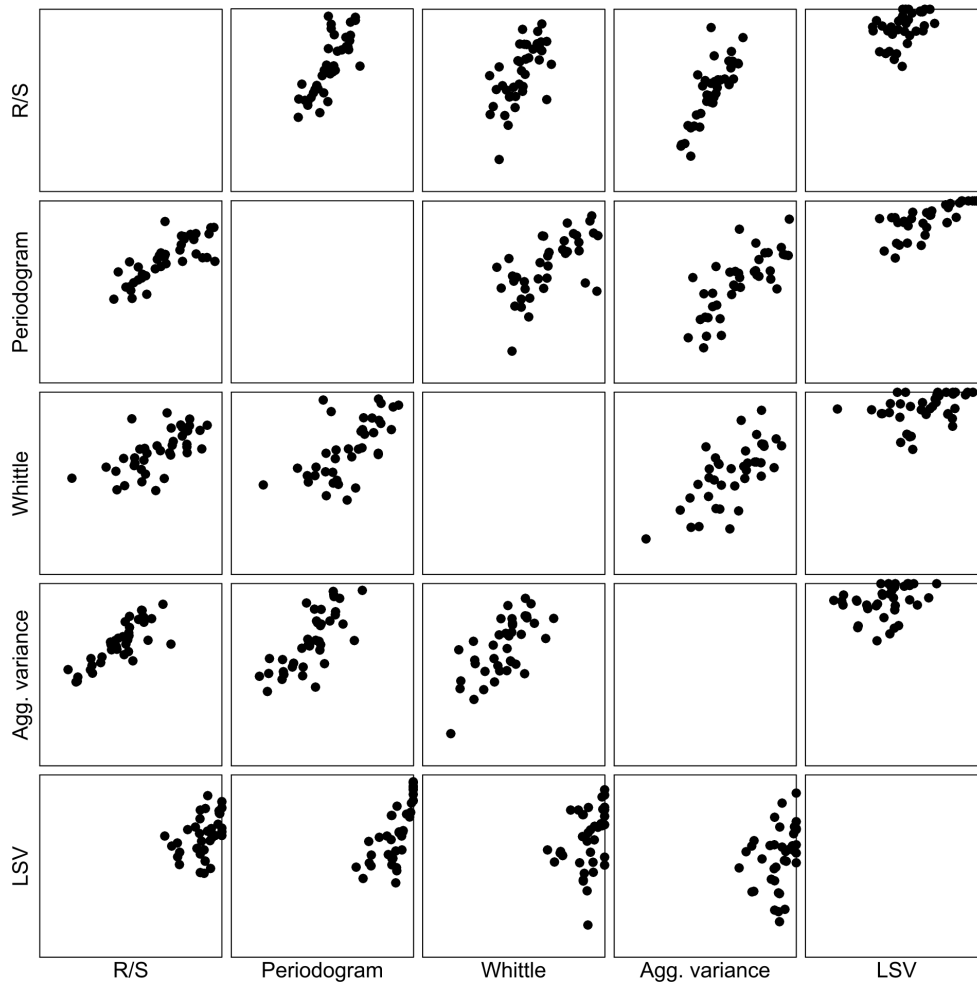


Figure 3.4: Scatter plots of the Hurst coefficients of daily runoff estimated by different estimation methods. Range of the axes is from 0.5 to 1 in all cases.

Table 3.4: Deviations of the H estimates of daily runoff for each estimation method from the mean of all estimators in terms of root mean squared error.

	R/S	Periodogram	Whittle	Agg. Variances	LSV
RMSE	0.058	0.042	0.047	0.107	0.137
Estimate mean	0.77	0.85	0.82	0.72	0.95

where n is the number of data sets and \bar{H}_{all} is the average H_i of all estimators. The $RMSE^{est}$ values are shown in Table 3.4. For R/S, periodogram and the Whittle estimators the $RMSE^{est}$ are smaller than 0.06, making the estimators almost equivalent with respect to this measure. LSV and aggregated variances estimates are shifted compared to estimates obtained by the other methods (LSV estimates being generally higher and aggregated variances estimates being lower than the estimation averages), while the remaining estimators are more consistent.

All further evaluations will be done for all estimation procedures. The illustrative figures, however will be presented for the periodogram method, which has the least RMSE, and the Whittle estimator. The Whittle estimator figures are included since it is possible to estimate confidence intervals for this method to illustrate the uncertainty of the Hurst coefficient estimates. The calculation of the confidence bounds does not incorporate the uncertainties in the estimator assumptions (such as normal distribution), thus the real confidence bounds would be wider than those calculated as part of the Hurst coefficient estimation.

3.4.2 Correlation between Hurst coefficient and catchment attributes

Plots of the Hurst coefficient estimated by periodogram regression and the Whittle method against the catchment attributes are shown in Figures 3.5 and 3.6.

The figures for the two methods are rather similar, which is in accordance with the high correlation between the H of the two estimators (Kendal's $\tau = 0.47$ and Spearman's $\rho = 0.64$; Tables 3.2 and 3.3). In the case of the Whittle estimator, the 95% confidence intervals as described in Appendix 2.1 are plotted. The confidence intervals indicate that the correlations are not just an artifact of the sampling uncertainty. Figures 3.5 and 3.6 are complemented by calculating Kendall's τ and Spearman's ρ for all estimation methods and all catchment attributes (Tables 3.5, 3.6).

The correlations between the Hurst coefficient and the catchment attributes are mostly consistent for all methods of estimation. The least consistent method is LSV which gives somewhat different results for a number of catchment attributes (eg. seasonality).

Figure 3.5 shows an almost linearly increasing dependency between H and catchment area. This effect is not so pronounced when considering the Whittle estimator on Figure 3.6. However, for all estimation methods such a positive correlation was tested as significant. Both figures show that H also increases with mean annual air temperature. Indeed, both correlation measures confirm the dependency as significant for all estimation methods except LSV. A decreasing dependence between H and mean annual precipitation P_i can be seen in Figures 3.5 and 3.6. However, the significance of this dependence was

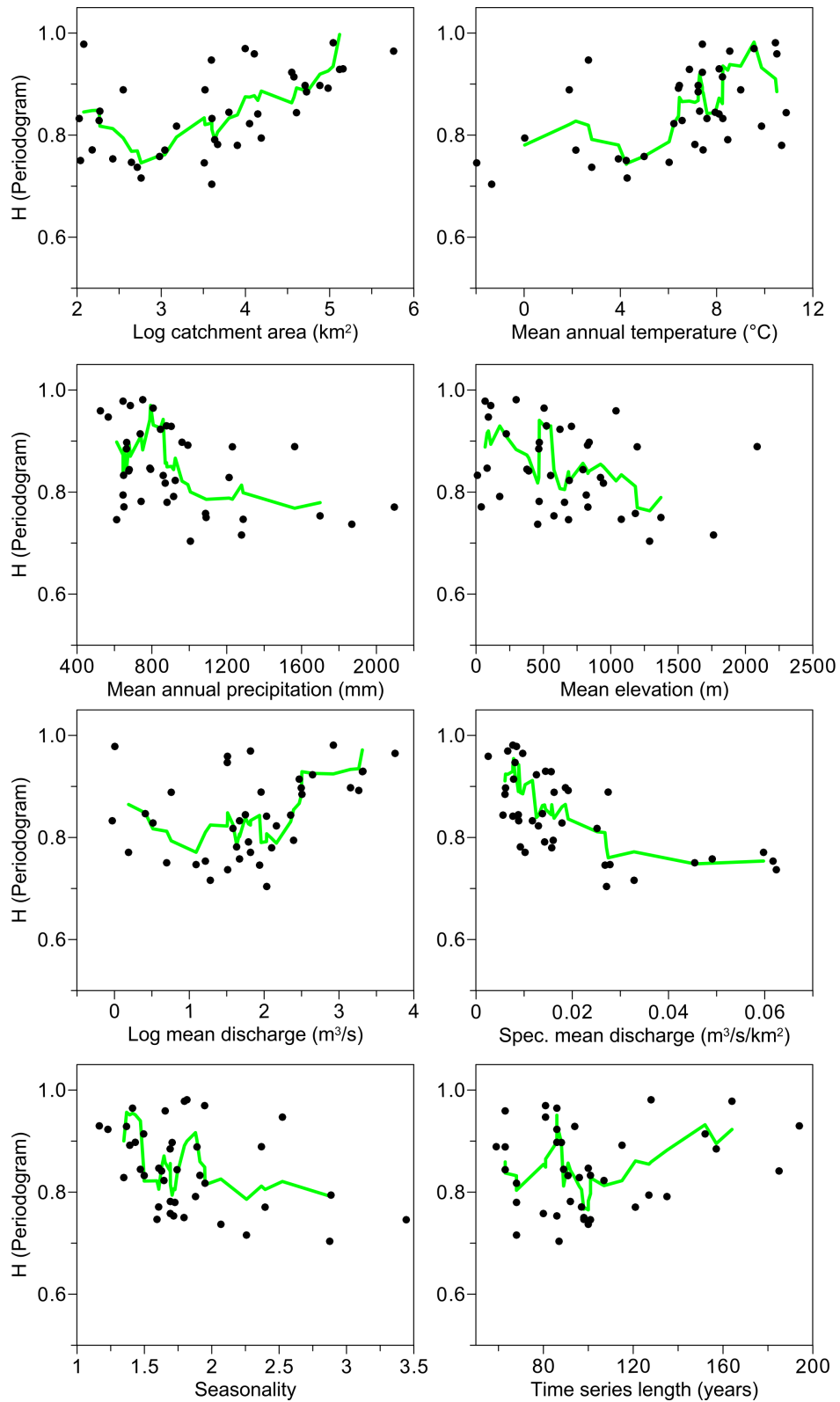


Figure 3.5: Dependency of the Hurst coefficient of daily runoff (estimated using the regression on periodogram) on catchment area, mean annual air temperature, mean annual precipitation, elevation, mean discharge, specific mean discharge, seasonality of runoff (maximum Pardé coefficient) and the length of the runoff time series. The green line represents a moving average over 5 data points.

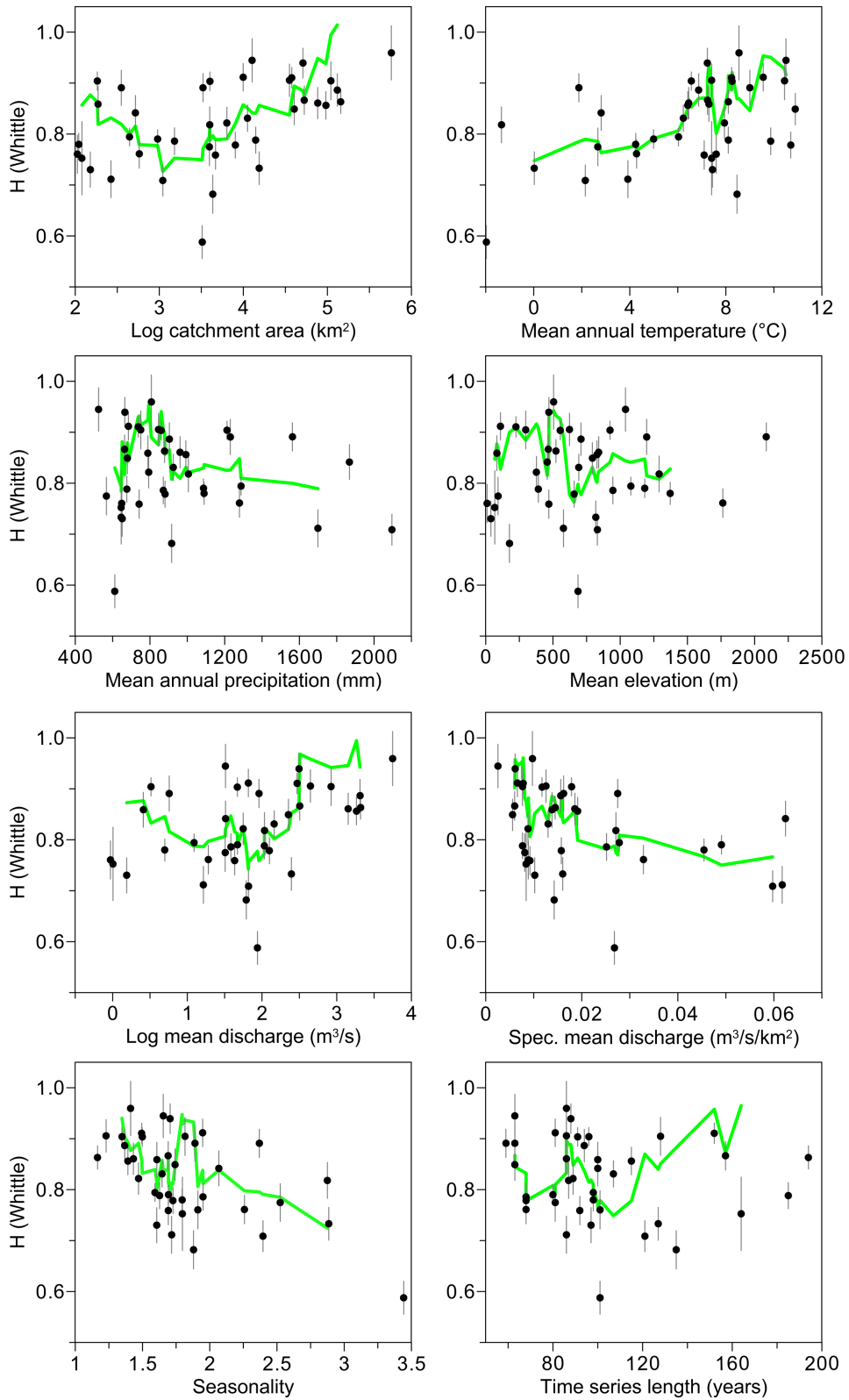


Figure 3.6: Dependency of the Hurst coefficient of daily runoff (estimated using the Whittle method) on catchment area, mean annual air temperature, mean annual precipitation, elevation, mean discharge, specific mean discharge, seasonality of runoff (maximum Pardé coefficient) and the length of the runoff time series. Bars indicate 95% confidence intervals of H . The green line depicts a moving average over 5 data points.

Table 3.5: Kendall's τ correlations between Hurst coefficients of daily runoff and catchment attributes. Those τ , where the independence hypothesis was rejected on a 95% level are printed in bold. Rightmost column shows the average τ over all estimation methods.

	R/S	Period.	Whittle	Agg. Var.	LSV	Average
Log catchment area	0.31	0.40	0.35	0.28	0.42	0.35
Mean ann. temp.	0.35	0.34	0.31	0.51	0.14	0.33
Mean ann. precip.	-0.18	-0.30	-0.04	-0.15	-0.37	-0.21
Elevation	-0.12	-0.26	-0.04	-0.02	-0.34	-0.14
Log mean discharge	0.21	0.29	0.29	0.20	0.35	0.26
Spec. mean disch.	-0.43	-0.47	-0.29	-0.38	-0.42	0.40
Seasonality	-0.33	-0.27	-0.35	-0.25	-0.14	-0.27
Time series length	-0.08	-0.00	-0.14	-0.23	0.15	-0.06

Table 3.6: Spearman's ρ correlations between Hurst coefficients of daily runoff and catchment attributes. Those ρ , where the independence hypothesis was rejected on a 95% level are printed in bold. Rightmost column shows the average ρ over all estimation methods.

	R/S	Period.	Whittle	Agg. Var.	LSV	Average
Log catchment area	0.45	0.54	0.52	0.45	0.56	0.51
Mean ann. temp.	0.47	0.51	0.41	0.65	0.24	0.46
Mean ann. precip.	-0.26	-0.44	-0.02	-0.22	-0.56	-0.30
Elevation	-0.19	-0.36	-0.07	-0.03	-0.50	-0.21
Log mean discharge	0.34	0.38	0.42	0.33	0.44	0.38
Spec. mean disch.	-0.60	-0.67	-0.40	-0.55	-0.60	-0.57
Seasonality	-0.45	-0.36	-0.48	-0.34	-0.20	-0.37
Time series length	0.11	0.02	-0.23	-0.32	0.21	-0.08

confirmed only for the periodogram regression and LSV method (for both Kendall's τ and Spearman's ρ). No clear dependence between the Hurst coefficients and elevation can be seen on Figure 3.6 (the Whittle estimator). A weak decreasing dependence on the elevation can be seen for the periodogram estimator on Figure 3.5. These graphical results are in accordance with the significance of the correlations measures. Both Kendall's τ and Spearman's ρ are close to zero (< 0.07 in absolute value) for the R/S, Whittle and aggregated variance estimators. On the other hand, the periodogram and LSV methods show significant correlations between the Hurst coefficient and elevation.

With regards to the runoff related catchment attributes, a moderate degree of dependence between H and the mean discharge (log) can be seen in Figures 3.5 and 3.6 for both methods. This is in accordance with the correlations in Tables 3.5 and 3.6. Unlike for the other catchment attributes, here the two correlation measures give significantly different results. Kendall's τ ranges between 0.20 and 0.35 (not significant for R/S and aggregated variance) and indicates a lower degree of correlation than Spearman's ρ which ranges between 0.33 and 0.44 where all methods show significant correlations. When the discharge is standardized by the catchment area (specific discharge), the correlations to the Hurst coefficient become more pronounced. The correlations are negative and relatively strong with Spearman's ρ ranging between -0.40 and -0.67. H slightly decreases with the seasonality expressed as the maximum Pardé coefficient (this coefficient was calculated from nondeseasonalized monthly mean runoffs). This weak to moderate negative correlation is statistically significant for all except the LSV estimator. There is very little correlation between H and the length of the runoff time series with the exception of Spearman's $\rho = 0.21$ for LSV and both correlation coefficients for the aggregated variance ($\tau = 0.23, \rho = 0.32$) method. The figures do not show any dependence between the Hurst coefficient and the time series length either.

The correlations described above should be in general interpreted carefully. The correlations do not include information about the actual causality between the runoff and the analyzed climate and storage based factors. Further interpretation should be made under consideration of the physical processes in the catchment and the correlations between the distinct catchment attributes (see Tables 3.8, 3.7). For example it can be seen that elevation and precipitation are rather strongly positively correlated, thus a question arises, whether the long term dependence in runoff is (partially) caused by elevation, precipitation or rather the combination of these two factors.

3.5 Discussion and conclusions

The main objective of this study was to analyze correlations between the Hurst coefficient as a measure of long range dependence and various climate and storage related catchment attributes. As a first step, Hurst coefficients were estimated for 39 European daily river discharge time series. For all estimators the Hurst coefficients were larger than 0.5. This is in accordance with (Koscielny-Bunde et al., 2006), another large scale study analyzing daily discharges, where long range dependence was detected in runoff. When considering those gauges, for which H was estimated in both studies, both (Koscielny-Bunde et al., 2006) and this analysis find $H > 0.8$ in the majority of cases. The only exception is the Severn at Bewdley, where the estimated values differ by almost 0.2. This may be related

Table 3.7: Kendall's τ correlations between the catchment attributes. Those τ , where the independence hypothesis was rejected on a 95% level are printed in bold. $\log(A_i)$ is the log of the catchment area, T_i and P_i are the mean annual temperature precipitation respectively, E_i is the mean catchment elevation, $\log(\bar{Q}_i)$ and q_i are the log mean and specific discharge, Pk_i is the seasonality expressed by the Pardé coefficient and N_i is the time series length in years.

	$\log(A_i)$	T_i	P_i	E_i	$\log(\bar{Q}_i)$	q_i	Pk_i	N_i
Log catchment area	1	0.17	-0.17	-0.03	0.82	-0.31	-0.26	0.07
Mean ann. temp	0.17	1	-0.26	-0.24	0.05	-0.46	-0.24	-0.09
Mean ann. precip	-0.17	-0.26	1	0.45	-0.03	0.64	-0.03	-0.13
Elevation	-0.03	-0.24	0.45	1	0.05	0.43	0.07	-0.32
Log mean discharge	0.82	0.05	-0.03	0.05	1	-0.13	-0.19	0.08
Spec. mean disch.	-0.31	-0.46	0.64	0.43	-0.13	1	0.12	-0.07
Seasonality	-0.26	-0.24	-0.03	0.07	-0.19	0.12	1	-0.1
Time series length	0.07	-0.09	-0.13	-0.32	0.08	-0.07	-0.1	1

Table 3.8: Spearman's ρ correlations between the catchment attributes. Those ρ , where the independence hypothesis was rejected on a 95% level are printed in bold. $\log(A_i)$ is the log of the catchment area, T_i and P_i are the mean annual temperature precipitation respectively, E_i is the mean catchment elevation, $\log(\bar{Q}_i)$ and q_i are the log mean and specific discharge, Pk_i is the seasonality expressed by the Pardé coefficient and N_i is the time series length in years.

	$\log(A_i)$	T_i	P_i	E_i	$\log(\bar{Q}_i)$	q_i	Pk_i	N_i
Log catchment area	1	0.30	-0.24	-0.04	0.94	-0.44	-0.38	0.10
Mean ann. temp.	0.30	1	-0.33	-0.33	0.10	-0.63	-0.34	-0.12
Mean ann. precip.	-0.24	-0.33	1	0.58	-0.05	0.80	-0.04	-0.18
Elevation	-0.04	-0.33	0.58	1	0.08	0.59	0.11	-0.46
Log mean discharge	0.94	0.10	-0.05	0.08	1	-0.19	-0.29	0.14
Spec.mean disch.	-0.44	-0.63	0.80	0.59	-0.19	1	0.23	-0.11
Seasonality	-0.38	-0.34	-0.04	0.11	-0.29	0.23	1	-0.15
Time series length	0.10	-0.12	-0.18	-0.46	0.14	-0.11	-0.15	1

to different record lengths in the two studies and different estimation method used. In general, a lower bound for the Hurst coefficient of approximately 0.6 is found in both studies.

Spearman's ρ and Kendall's τ were used to compare the estimators between each other, obtaining significant positive correlations. This indicates that the estimation results are consistent, even if we cannot verify how far they are varying from the real Hurst coefficients of the data. In order to obtain as realistic results as possible, we deseasonalized the data prior to the analysis, thus avoiding systematic errors which the periodogram and R/S estimators produce in presence of seasonality (Montanari et al., 1999b). The strong correlation between R/S and the periodogram regression ($\tau = 0.62, \rho = 0.80$) is in accordance with an economic study, comparing these two methods on stock returns (Blasco and Santamaría, 1996).

Rather than in the exact value of H , we were interested in the strength of the long range dependence compared to those of the other catchments in the study. Since the estimators gave sufficiently consistent results, it was possible to conduct an analysis of the correlations between Hurst coefficients (indicating the strength of the long range dependence) and the selected catchment attributes.

For this purpose eight catchments attributes such as area, elevation, precipitation, and temperature were used. For each of them, Spearman's ρ and Kendall's τ correlations between H and the respective catchment attribute were calculated. The dependencies between the Hurst coefficient and the catchment attributes were mostly consistent for all methods of estimation. The analysis showed that the strength of the long range dependence does not significantly depend on the elevation and time series length. Positive dependence was found for mean discharge, catchment area and mean annual temperature. On the other hand, long range dependence depends negatively on mean specific discharge, mean annual precipitation and seasonality. The correlation between mean annual precipitation and the Hurst coefficient was significant only for estimates obtained by two of the applied estimation methods. These results are in general agreement with the results of (Gudmundsson et al., 2011), who analyze correlations of low frequency components of runoff. Both studies found significant negative correlations between mean precipitation/mean runoff (standardized by area) and the low frequency component of runoff (meaning high Hurst coefficients in our case). Positive correlations with air temperature are in accordance with this study as well. The positive correlation with catchment area is in accordance with (Mudelsee, 2007).

No significant correlation was found between the time series length and the Hurst coefficient. This might imply that the drawbacks of the Hurst coefficient estimation procedures are not due to data scarcity, rather than due to imperfect choice of the estimation method or the unknown properties of the measured runoff.

The hydrological interpretations of the results can be discussed in terms of catchment area effects, catchment wetness, and snow processes. Catchment area effects are reflected by two attributes, catchment area itself and river discharge which is highly correlated with catchment area. The positive correlations of H with both attributes suggest that catchment storage will strongly affect the long range dependence of runoff. One may expect larger storage in larger catchments, both due to groundwater (particularly during low flow periods) and inundations (particularly during flood periods). Indeed, catchment response times tend to increase with catchment area (eg. Gaál et al. (2012)). The long

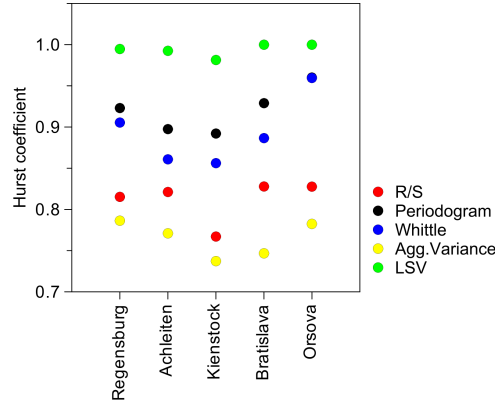


Figure 3.7: Hurst coefficients of daily runoff for the stations at the Danube River. Stations are ordered according to their position on the river, Regensburg being the closest to the spring of the Danube and Orsova the most downstream of the stations analyzed.

term component of stream flow variability is relatively more important compared to the short term component when the Hurst coefficient is high. This may be caused by the large storage capacities of a catchment. To examine this effect in more detail Figure 3.7 shows H for five stations at the Danube. There is no clear increasing trend of H with the position in the stream. This may be due to the size and complexity and the number of anthropogenic influences in the Danube basin. Further explanatory factors might be the high correlations between the discharges of the Danube stations.

Catchment wetness effects are reflected by mean annual precipitation and mean specific discharge. The negative correlations of H with both attributes suggest wet catchments exhibit low Hurst coefficients while dry catchments exhibit large Hurst coefficients. Apparently, for wet catchments the short term variability is stronger than the long term variability. In contrast, in dry catchments there is stronger variability on a long term scale. This is not surprising for two reasons. Wet catchments tend to have frequent rainfall events without a clear low flow season which increases the short term variability relative to dry catchments. Also, in dry catchments the between year variability of streamflow may be relatively large as runoff is more sensitive to rainfall fluctuations than in wet catchments (Harman et al., 2011).

Snow processes are reflected by air temperature and the seasonality index. The positive correlations of H with air temperature and the negative correlations of H with the seasonality (maximum Pardé coefficient) suggest that snow dominated areas (low air temperature, large seasonal runoff fluctuations and therefore large seasonality) have less long range dependence (and more short term fluctuations) than catchments where snow processes are less important. Apparently, a snow dominated stream flow regimes tends to smooth out the fluctuations between years while there is significant short term variability that deviates from the mean seasonal variation.

The findings of this study have important implications for stochastic hydrological modelling especially in water resources management and reservoir operation. For example in order to determine the supply risk from a reservoir, long term perspective is of interest, thus the long range dependence needs to be incorporated into the model. This study suggests that, depending on the climate and catchment characteristics, these types of models

needed to be parameterised in a different way. From a more theoretical perspective it is also of interest to identify the main factors related to climate and storage that influence the long range dependence of stream flow at a regional scale.

Chapter 4

Long term variability of the Danube River flow and its relation to precipitation and air temperature

Abstract

In this work the long cycles and long range dependence of monthly discharge, precipitation and air temperature time series from the Danube River during the years 1901 - 2006 were analysed using wavelet analysis, with emphasis on wavelet coherence and cross wavelet spectra. All time series were deseasonalized prior to the analysis. Long cycles with 11 - 15 year periods during almost the whole observed period in discharge and during 1935 - 1975 in precipitation were found. Furthermore a reappearing four year cycle was found in all discharge time series. No significant long cycles were found in the temperature time series, which on the other hand display long term persistence. The cross - wavelet spectra and the wavelet coherence show strong correlation between the precipitation and discharge spectra in the low frequency intervals. Furthermore, a convolution of precipitation and catchment response function was used to examine the propagation of long cycles from precipitation to discharge. The results show, that the long range dependence in precipitation propagates into discharge and that the precipitation lead in the cross - wavelet spectrum increases with the increasing response time. The results indicate that especially mean monthly precipitation could be used as input variable in order to improve stochastic discharge modelling.

4.1 Introduction

Studies analysing the effect of climate related drivers, such as precipitation and air temperature on discharge are important in order to increase the understanding of the interactions of such process, especially for construction of stochastic models representing long term discharge fluctuations. Within the framework of the ongoing climate change debate, the number of studies analysing the influence of various climate and storage related drivers on discharge has increased in the past years (Blöschl and Montanari, 2010) as a result of the increased interest in the behaviour of discharge over long time scales in

general.

Multi - annual cycles and trends have been identified in discharge time series by various methods - filtering techniques and spectral analysis (Pekárová et al., 2003, Probst and Tardy, 1987) or wavelet analysis (Labat, 2008, Sang, 2013). Many studies focused on capturing and describing periodical behaviour of processes from a long term perspective use wavelet analysis. (Timuhins et al., 2010), for example found long cycles of 4, 11 and 30 years in Baltic rivers in the past century. (Massei et al., 2010) found 5 - 7 and 17 years cycles in both daily discharge and precipitation for the River Seine in France. (Markovic and Koch, 2013) examined discharge, precipitation and other variables on several stations for the Elbe River in Germany, finding long cycles in mean monthly discharge and precipitation, but not in temperature. (Andreo et al., 2006) found long cycles with periodicities of 2-3 and 4-6 years in monthly precipitation and temperature time series on the Southern Iberian Peninsula. Similarly (Ouachani et al., 2013) found 2-3 and 4-8 years cycles in the seasonal precipitation of Tunisian rainfall.

Several authors examine the influence of climate phenomena, such as the North Atlantic Oscillation on discharge and precipitation. For example (Rimbu et al., 2002) finds, that decadal variations between discharge and precipitation in the lower Danube Basin are "in good agreement" and are "largely controlled" especially by NAO. (Mann et al., 1995) find, that decadal atmospheric circulation have high influence on Great Salt Lake levels through precipitation. (Markovic and Koch, 2013) find significant connection between NAO and mean monthly precipitation on the Elbe River in Germany. At a broader European and Atlantic scale, the influence of NAO on precipitation averages is also well known (Hurrell, 1995, Osborn et al., 1999, Rogers, 1997). More recently, the non-normality and nonlinearity in the multidecadal response of precipitation to NAO have been analysed by Pires and Perdigao (2007) for a large swath of the Northern Hemisphere spanning from the Eastern US to Western Asia. NAO impacts on precipitation have been identified even in regions where the quantities are linearly uncorrelated. However, studies focusing on the influence of precipitation and air temperature on discharge using wavelet analysis are scarce, even though precipitation and temperature are most relevant for hydrological predictions as well (Blöschl and Montanari, 2010). (Liu et al., 2011) analyzed rainfall and runoff at a half - hourly time step in four experimental catchments in Northwestern China and found the wavelet power spectra of rainfall and runoff to be highly correlated. Another characteristic used to describe the long term behaviour of time series is long range dependence, i.e. when the autocorrelation function remains significant even for long lags. Long range dependence has been found in daily discharge of European rivers (Mudelsee, 2007, Szolgayova et al., 2013) and daily precipitation time series in Malaysia (Yusof et al., 2013). (Skoien et al., 2003) found no long range dependence for precipitation data and some slight long range dependence for discharge in Austria. However, studies examining the relationship between long range dependence and presence of long cycles are lacking.

In order to capture the long term behaviour in discharge modelling knowledge of the long term properties of the time series is of importance. A wide range of stochastic models reflecting the complexity of geophysical processes such as changes in the regime (Bataglia and Protopapas, 2011, Komorníková et al., 2008, Valent et al., 2011), long term persistence (Frolov, 2011, Montanari et al., 2000) or heteroscedasticity (Elek and Markus, 2007, Modarres and Ouarda, 2013) exist. Within the modelling framework, the challenge

is to connect the complexity contained in the mathematical models to processes and external drivers (Fisher et al., 2012, Gelati et al., 2010, Lee, 2012). (Mann et al., 1995) suggests, that modelling and especially forecasting may be improved, when low frequency events would be more considered in the models. In order to increase the quality of such stochastic models, especially when interested in more process based multivariate models including climate and storage related variables, the interaction of discharge and its drivers needs to be examined as a function of time including long range dependence.

The aim of this paper is to analyze precipitation, air temperature and discharge time series from the upper part of the Danube River in southern Germany, Austria and Slovakia in order to gain understanding of low frequency fluctuations and their interactions and thus explore, whether and how these drivers (especially in monthly time step) could be incorporated into a multivariate discharge model. The following questions will be addressed: What are the statistical characteristics of discharge, precipitation and air temperature as a function of time and do these time series display long range dependence? At what scales and when do the data fluctuate? How are the cycles in discharge related to those in precipitation and temperature?

4.2 Data and methods

The analysis was performed on four data sets, each consisting of a discharge, precipitation and air temperature time series. The discharge time series from the stations Hofkirchen, Achleiten, Kienstock and Bratislava with catchment areas ranging between from 47000 to over 131000 km^2 were used in the analysis (further descriptive statistics including the Hurst coefficient estimates are listed in Table 4.1).

In order to analyse long term behaviour long series of records are necessary. Thus only series, where sufficiently long precipitation, temperature and discharge data sets are available were used. All time series cover the period between November 1901 and October 2006 (105 years). A monthly time step was used in the analysis. The discharge time series were provided by the Global Runoff Data Center (GRDC, 2011). The precipitation and temperature time series used for analysis were calculated based on data obtained from the European Climate Assessment and Dataset (ECA&D) (Tank et al., 2003). The geographical positions of all stations are shown in Figure 4.1.

For each discharge time series catchment area average precipitation time series were constructed using Thiessen polygons (Dingman, 2008). Since the number of available stations changes over time, for the sake of consistency only 16 precipitation stations with sufficiently long records were used for estimating the catchment area averages.

The mean catchment air temperature time series were obtained by linear regression performed for each day of the analyzed period, temperature being the dependent and elevation the explanatory variable. The resulting temperature time series were calculated based on the fitted regression coefficients (for each day) using the mean elevation of the respective catchment area. The monthly series were aggregated from thus obtained daily regression series.

No deterministic trend was found in any of the discharge or precipitation time series. Significantly increasing trends were found in all of the temperature series. However, the wavelet analysis and Hurst coefficient estimation results listed and discussed later were

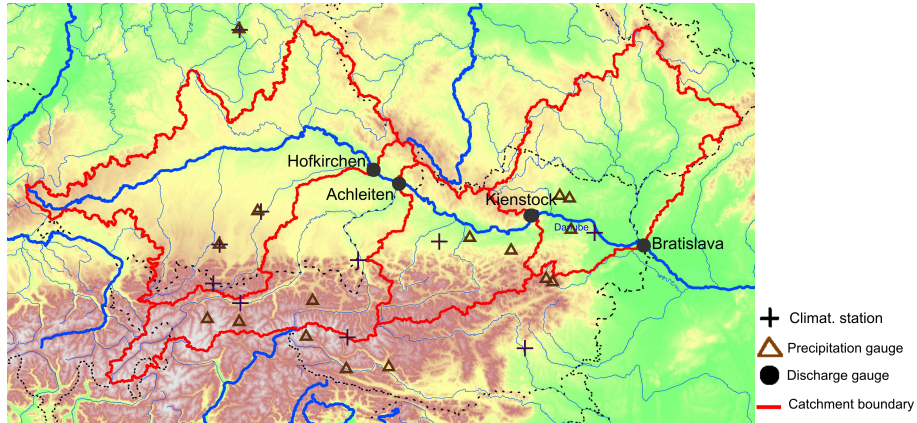


Figure 4.1: Geographical position of discharge, precipitation and climatological gauges including the catchment area boundaries.

conducted on the non-detrended series, since it can not be distinguished, whether the trend found in the analysed time series is only a part of a cycle with frequency too low to be detected in the data set due to its limited length. It should be noted, that the DFA method already accounts for such trends, thus detrending would not have any effect on the Hurst coefficient estimates using this method. The regression on the periodogram produced significant Hurst coefficient estimates for both detrended and non-detrended time series and the wavelet and crosswavelet spectra were almost trend invariant.

All the time series were deseasonalized prior to further analysis (see chapter 2).

The catchment average precipitation and air temperature series will be referred to as temperature and precipitation time series in the following for the sake of brevity.

Table 4.1: Data description for the four data sets sorted according to the discharge gauge. All four discharge gauges are on the Danube River. For all time series of monthly data the time interval November 1901 - October 2006 (105 years) was used. The descriptive statistics are given for non-desaseasonalized data. The Hurst coefficients were estimated using the regression on periodogram and the detrended fluctuation analysis (DFA).

	Hofkirchen	Achleiten	Kienstock	Bratislava
General description				
Country	Germany	Germany	Austria	Slovakia
Catchment area, km^2	47496	76653	95970	131331
Latitude	48.68	48.58	48.38	48.14
Longitude	13.12	13.50	15.46	17.11
Elevation, m	631.06	839.97	827.55	708.63
Descriptive statistics - Discharge				
Mean, m^3s^{-1}	640.72	1426.24	1849.54	2056.38
Standard deviation, m^3s^{-1}	243.85	537.98	706.60	800.87
Coefficient of variation	0.38	0.38	0.38	0.39
Hurst coeff. - Period.reg.	0.74	0.71	0.60	0.63
Hurst coeff. - DFA	0.73	0.70	0.67	0.67
Descriptive statistics - Precipitation				
Mean, mm	2.52	2.65	2.64	2.38
Standard deviation, mm	1.41	1.41	1.37	1.25
Coefficient of variation	0.56	0.53	0.52	0.53
Hurst coeff. - Period.reg.	0.66	0.55	0.51	0.43
Hurst coeff. - DFA	0.56	0.51	0.51	0.50
Descriptive statistics - Temperature				
Mean, $^{\circ}C$	7.86	7.06	6.81	7.45
Standard deviation, $^{\circ}C$	7.06	6.90	6.91	7.00
Coefficient of variation	0.90	1.02	1.02	0.94
Hurst coeff. - Period.reg.	0.72	0.71	0.71	0.72
Hurst coeff. - DFA	0.65	0.65	0.65	0.65

4.2.1 Discharge convolution

In order to help interpret the relationship between precipitation and discharge and the propagation of low frequency events, a simple convolution calculating discharge from precipitation was constructed. Changing the properties of the convolution function allows to modify the properties of the discharge time series based on a chosen precipitation time series as desired and examine the changes in the cross - wavelet spectrum and the changes in the wavelet coherence. Thus the dependence of discharge on precipitation for different frequencies and time windows can be examined. For this purpose, a daily time step was used. The daily precipitation time series display long range dependence, whereas the monthly precipitation time series behave similarly to a random noise series (see Table 4.1 and Section 4.3.1). Thus the use of daily precipitation allows a comparison of the spectra and Hurst coefficients in terms of the long term persistence in precipitation. This would

not be possible if monthly series was used.

Discharge series were calculated from precipitation time series for the Hofkirchen and Bratislava by

$$Q_t^{gen} = P_t * (\alpha_1 e^{-\alpha_1 t} w_1 + \alpha_2 e^{-\alpha_2 t} w_2) = \int_{-\infty}^{\infty} P_\tau (\alpha_1 e^{-\alpha_1(t-\tau)} w_1 + \alpha_2 e^{-\alpha_2(t-\tau)} w_2) d\tau \quad (4.1)$$

where Q_t^{gen} , $i = 1, 2$ is the calculated discharge series, $*$ is a convolution, P_t is the precipitation series, α_i indicate different travel times of water in the catchment and w_1, w_2 are weights of the respective travel times with $w_1 + w_2 = 1$. Two different travel times with different weights were used in order to simulate a short term (high frequency, short travel time) and a long term (low frequency, long travel time) component of the discharge. In all cases a convolution kernel representing 10 days travel time was combined with long travel time kernels - 1, 5 and 10 years. The long travel times were chosen to be similar to the long cycles found in discharge. Both time series were deseasonalized after the discharge generation analogically to the monthly data sets. The use of deseasonalized data justifies that snow and soil moisture are not represented in the convolution function.

4.3 Results

4.3.1 Long cycles

The graphical output from the global spectrum test can be seen on Figure 4.2, the respective spectra for the analysed variables can be found on Figure 4.5. On the 95 percent significance level several long cycles were detected for both discharge and precipitation time series. The global wavelet spectra of the discharge time series (Fig. 4.2 left) are above the red noise background spectrum for periods between 11-15 years for all stations except Bratislava. Cycles with approximately this periodicity are visible in the wavelet spectra for all stations for almost the whole duration of the analysed period. In Achleiten the cycle is significant all the time. Furthermore, for all stations a shorter cycle of 4 years was detected. Based on the wavelet spectra, this shorter cycle is significant only over shorter time periods, for example between the years 1910 - 1940 and later between 1960 and 1970. All time series display long range dependence with Hurst coefficients larger than 0.7 for the two German stations, and larger than 0.6 for Kienstock and Bratislava for both estimation methods. The Hurst coefficient estimates can be found in Table 4.1. All catchment precipitation time series contain a cycle with periods between 11 - 15 years, and on the upstream Hofkirchen station, a long 22 year cycle was detected (Fig. 4.2 middle). These cycles can be seen on the wavelet spectra as well, even though they vary over time. For all four stations, the 11 -15 year cycle is significant approximately between the years 1935 - 1975. Furthermore, at Hofkirchen, the 22 years cycles is detected as significant until the year 1955. However, the analysis of the autocorrelation functions of all these time series (not shown here) shows, that the autocorrelation structure, especially of the two downstream stations, is very close to white noise and the Hurst coefficients are close to 0.5 in almost all cases accordingly. The decrease of the Hurst coefficient as we move downstream on the Danube river (e.g. H for Hofkirchen is 0.66 and for Bratislava 0.43 using the regression on periodogram method) corresponds to the decrease in the

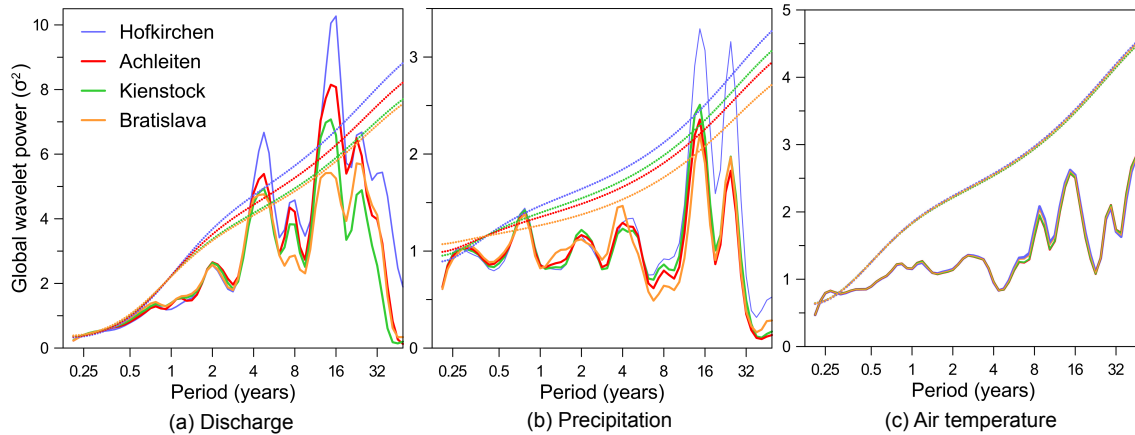


Figure 4.2: The global wavelet spectra of the discharge, precipitation and temperature time series. The dotted line represents the 95 percent confidence bound.

areas significant in power on the precipitation wavelet spectra. In general, the global wavelet spectra of the monthly station precipitation time series used for calculation of the catchment precipitation series show a varied behaviour (see Fig.4.3) depending on the geographic position of the climatic stations. Stations in the north east and south west of the considered region contain no significant long cycles. This has an impact on the catchment area averages interpolated from the station time series and on the resulting cycles detected.

The temperature time series do not contain any long cycles compared with the red noise background (Fig. 4.2 right). Even though the global wavelet spectrum did not indicate any significant cycles, a significant frequency of approximately 10 - 15 years can be seen from the wavelet spectra of all time series between the years 1935 - 1955. Furthermore, there is long range dependence present in all four time series: the Hurst coefficients are approximately 0.6 according to the detrended fluctuation analysis and 0.7 according to the regression on the periodogram method. The Hurst coefficients for all time series are almost identical, as are the wavelet spectra (see Fig. 4.5).

4.3.2 The cross - wavelet spectra and wavelet coherence

The cross - wavelet spectra and the wavelet coherence spectra can be found in Figures 4.5 and 4.6. The first two rows of Figure 4.6 display the cross - wavelet spectra of precipitation and discharge in the first row and temperature and discharge in the second row. The bottom two rows show the respective wavelet coherence spectra.

When comparing the cross - wavelet spectra with the wavelet spectra of the discharge time series, it can be seen that the significant areas of the cross - wavelet spectrum approximately copy the areas significant in the discharge spectra, rather than those of the precipitation spectra for all stations (compare rows one and two in Figure 4.5 with the first row of Figure 4.6). The time series have both high power for the periods of approximately four years for most of the observed time window. In this period range, precipitation leads discharge by approximately 45 degrees (corresponding to six months lead time) in the first half of the time series until the 1960s. Then, however, we can observe

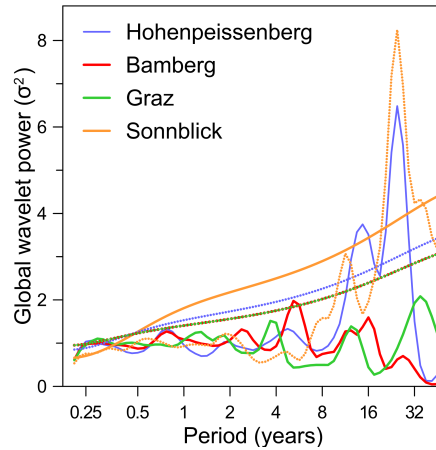


Figure 4.3: Example of the global wavelet spectra of mean monthly precipitation time series used for the calculation of the catchment average precipitation series. The dotted lines indicate the 95 percent confidence bounds of a red noise global wavelet spectrum.

a change in the behaviour for all four analysed data sets and the two time series are in phase until the end of the observation period. In the low frequency area, where the cycles of 11 - 14 years were observed, the two series are both high in power as well. It can be seen that the lead time of precipitation increases with increasing periodicity of discharge. Here the phase difference changes to almost 90 degrees, which would indicate approximately 3 years lead time. The discharge and precipitation time series show significant degree of coherence for all frequencies for most of the time for all four stations. The time series are almost in phase until the end of the observation period with a lead time of 1-2 months. In the low frequency there is a common area of no coherence for all data sets in the time window 1920 - 1970 for the period interval between 4 - 11 years.

The temperature spectra display a significant area of power between 1930 - 1960 with the periodicity around 11 years. This time period corresponds to years, where daily air temperature minima were generally below the long time average (compare with an example of the Hofkirchen temperature time series on Fig. 4.4). This means that the long cycles were present for years with especially cold winters.

A major difference between the temperature - discharge and precipitation - discharge relationships can be seen in the wavelet coherence spectra. The precipitation time series show high levels of coherence for most frequencies and times. On the other hand, the coherence between temperature and discharge is less pronounced at most frequencies and is significant only in the low frequency range. In the temporal periods where the wavelet coherence and the cross - wavelet spectra are significant compared to the red noise background, the temperature and discharge are in anti - phase (20 years periodicity), with increasing period temperature leads discharge by approx. 225 degrees (approximately 13 years leading time). In other areas the phase shifts are random. The significantly coherent period ends in the late 1950s.

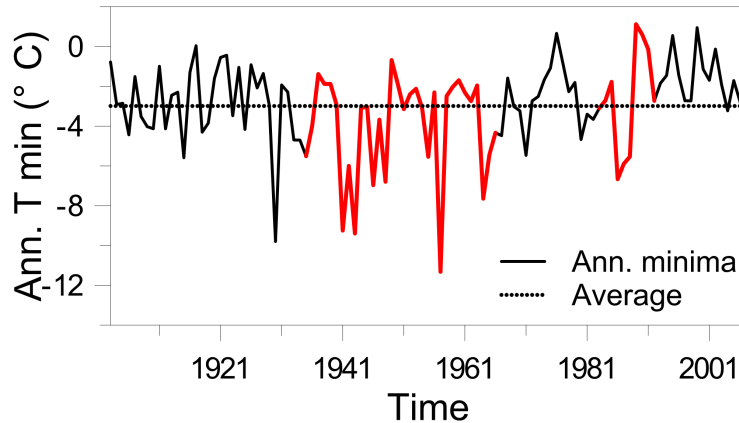


Figure 4.4: Daily minimum temperatures for each year for the Kienstock catchment average temperature time series. The red line indicates the time period, where the wavelet spectrum is significant in power for the low frequencies (over 5 years periodicity).

4.3.3 Convolved data

The goal of the convolution analysis was to gain understanding of the relationship between the long range dependence and the cyclical behaviour in the discharge found in the wavelet spectra. In order to achieve this, several daily discharge time series were calculated using the convolution function described in Section 4.2.1. Table 4.2 shows an overview of Hurst coefficients for some of the convoluted time series with various kernel combinations and weights of the kernels used. We see that the Hurst coefficients of the calculated discharge time series increase with the increase of the weight of the long time kernel component. Using only a very long travel time kernel yields a non-stationary process, thus the time series does not fulfill the assumptions of regression on the periodogram estimator, producing $H > 1$ for both estimation methods. The results indicate that the long range dependence in discharge is influenced by the presence of the long range dependence in precipitation (note, that on a 99 percent significance level the Bratislava precipitation time series does not display long range dependence). However, this influence is not very sensitive to the generator input parameters, since long range dependence was detected in all generated time series, independent of the weight combinations of the kernels. Assuming a convolution function with a dominant long time produces a non-stationary discharge output. Furthermore it seems that with decreasing the travel time of the long term kernel actually produces an increase in the Hurst coefficient. Thus, based on the convolution model, it is not possible to directly attribute the increase in Hurst coefficient to the presence of long cycles (represented by the long time kernel).

An example of the wavelet, cross-wavelet and wavelet coherence spectra of the generated data can be seen on Figure 4.7. The time series depicted on the figure was calculated using 5 years travel time with weight 0.9 combined with the 10 days travel time mentioned above, using the Bratislava precipitation time series. Here the estimated Hurst coefficient (using the DFA method) coincides with that of the measured Bratislava daily discharge series. The wavelet coherence is close to 1 for almost all the area of the spectrum. The areas of no significant coherence observed in the real precipitation/discharge time series

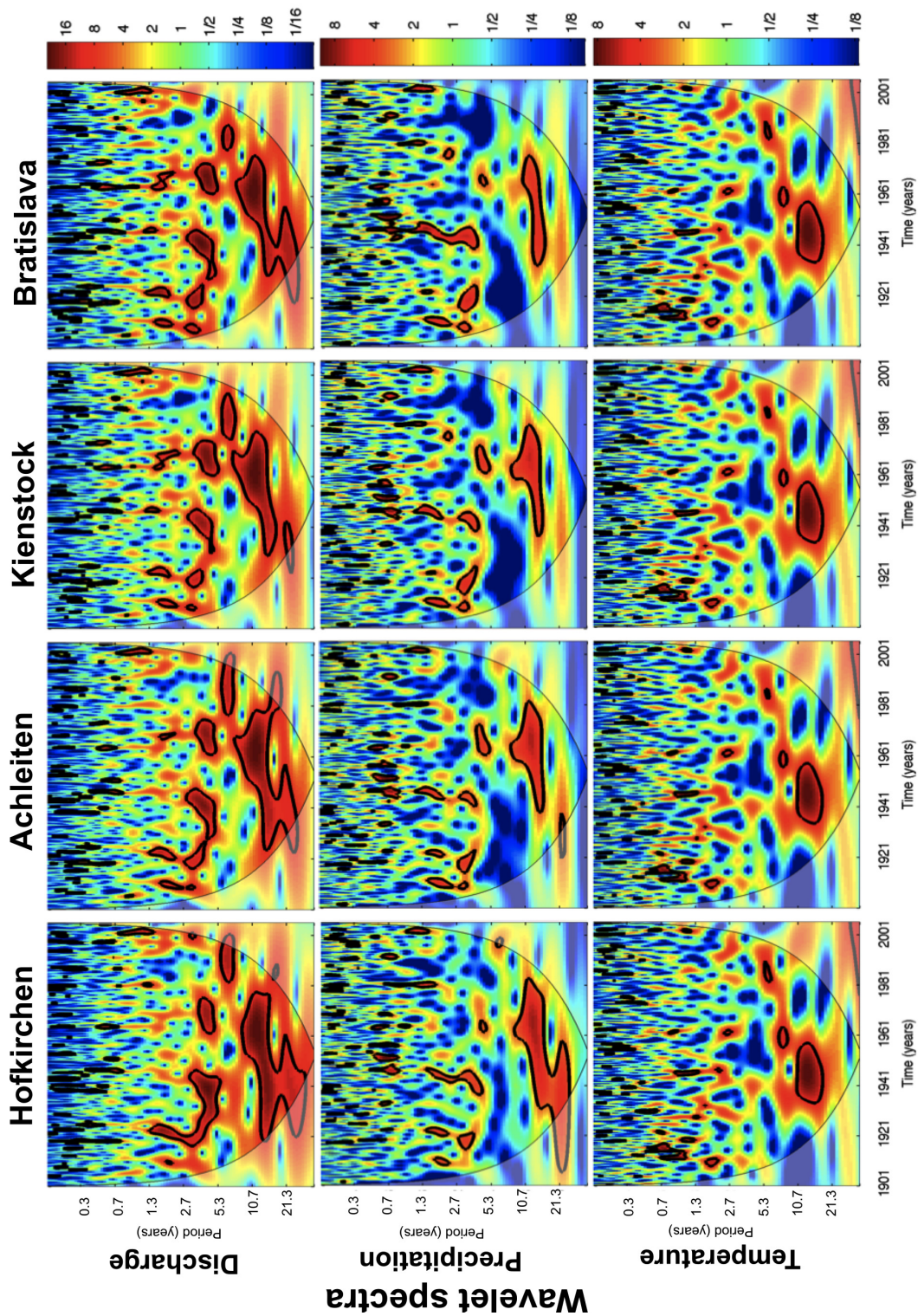


Figure 4.5: The wavelet spectra for each of the analysed variables - discharge, catchment average precipitation and air temperature.

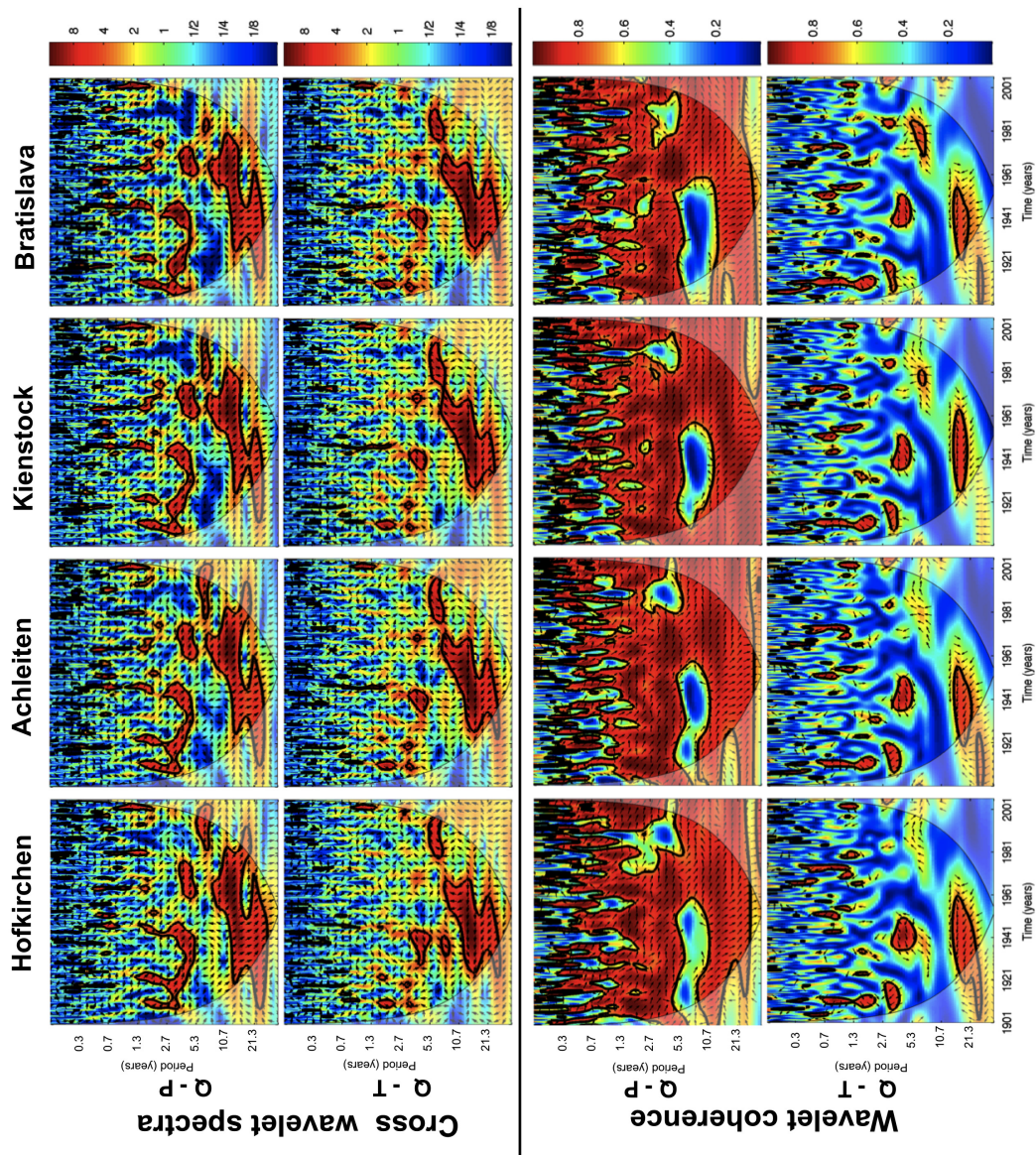


Figure 4.6: The cross - wavelet and wavelet coherence spectra. The first two rows show the cross - wavelet spectra between precipitation/discharge and air temperature/discharge respectively. The bottom two rows show the wavelet coherence spectra for the same pairs of variables. Arrows show the phase shift between the respective time series. Colours indicate the measure of coherence - red colour implies high degree of coherence. Arrows pointing right indicate that the two time series are in phase. Arrows pointing down indicate that precipitation/temperature leads discharge.

Table 4.2: Hurst coefficient estimates for daily convoluted discharge time series. The Hurst coefficients of the real precipitation and discharge time series are listed in the first two rows. Hurst coefficients for different weight combinations and different travel times are listed in the following rows. The Hurst coefficient was estimated using regression on periodogram (Per.Reg.) and detrended fluctuation analysis (DFA).

	Hofkirchen		Bratislava	
	DFA	Per.Reg.	DFA	Per.Reg.
Observed time series				
Discharge	0.91	0.89	0.88	0.89
Precipitation	0.56	0.57	0.54	0.55
Calculated discharge - travel times 10 days, 10 years				
$w_{1years} = 0$	0.76	0.76	0.73	0.73
$w_{1years} = 0.1$	0.76	0.76	0.74	0.73
$w_{1years} = 0.5$	0.77	0.78	0.75	0.74
$w_{1years} = 0.9$	0.85	0.85	0.83	0.80
$w_{1years} = 1$	1.27	1.47	1.24	1.42
Calculated discharge - travel times 10 days, 5 years				
$w_{5years} = 0.1$	0.76	0.77	0.74	0.73
$w_{5years} = 0.5$	0.77	0.78	0.76	0.75
$w_{5years} = 0.9$	0.83	0.86	0.88	0.87
$w_{5years} = 1$	1.06	1.37	1.24	1.42
Calculated discharge - travel times 10 days, 1 year				
$w_{10years} = 0.1$	0.77	0.77	0.74	0.74
$w_{10years} = 0.5$	0.80	0.82	0.81	0.79
$w_{10years} = 0.9$	0.93	1.04	1.03	1.06
$w_{10years} = 1$	1.06	1.36	1.22	1.41

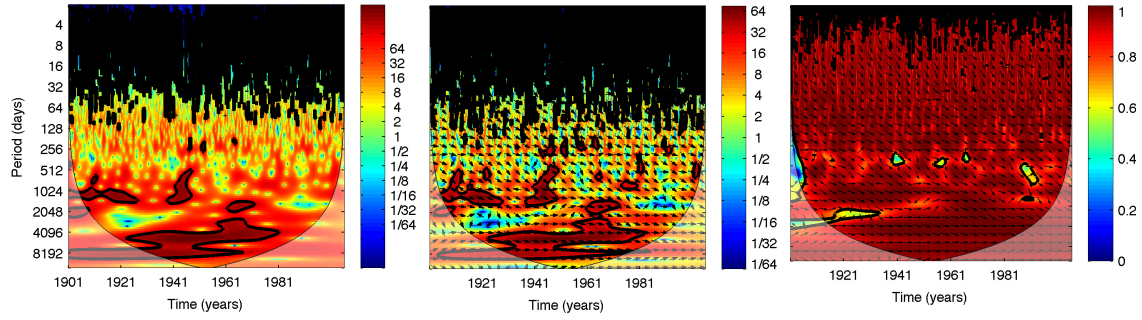


Figure 4.7: The wavelet (left), cross - wavelet (middle) and coherence spectra (right) for the discharge time series calculated from the Bratislava precipitation time series using the kernel combining 10 days and 5 years travel times with respective weights 0.1 and 0.9.

spectra could be only partially reproduced using this simple generator. The high wavelet coherence is mainly caused by the fact that the discharge time series were directly calculated from the precipitation time series, especially without any added noise. Similarly to the spectra of the observed precipitation/discharge time series, the phase arrows show that for shorter periodicities precipitation leads discharge. In these cases the phase is influenced by the travel time of the water in the catchment. However, the time variability of discharge for longer periods depends on the variability in the precipitation time series, rather than on the travel time. For periodicities bigger than the long time kernel, the phase arrows are not influenced by the weights of each of the kernels. However, for shorter periodicities the increase in lead time of precipitation increases with the increase of the weight of the long time kernel (not shown here).

4.4 Discussion and conclusions

The main goal of this paper was to analyse the long term behaviour of mean monthly discharge, temperature and precipitation time series of four stations on the Danube River, with emphasis on long cycles and the dependencies between precipitation, air temperature and discharge. Statistical tests of the global wavelet spectra confirmed a four year cycle in all observed discharge time series on a 95 percent significance level. Furthermore, long cycles of 11 - 15 years were detected on the three upstream stations. This is in agreement with (Labat, 2008), who found similar cycles (4, 14, 20 and 33 years) in the annual discharge of the Danube River at Ceatal Izmail in Rumania. It is as well in agreement with findings of other authors, who analysed European discharges and found long cycles - 4 and 11 years cycles on the Baltic rivers (Timuhins et al., 2010) and 10 - 14 years cycles on the Elbe River (Markovic and Koch, 2013). (Rimbu et al., 2002) points out that long cycles, such as those found in the analysed discharge time series are in correlation with positive phase of the NAO and can be associated with below the average sea surface temperature anomalies as well.

Unlike other authors, who found cycles of around 5 years in precipitation data sets on the Iberian Peninsula and North Africa (Andreo et al., 2006, Ouachani et al., 2013), only

a 11 - 13 year periodicity was detected in precipitation. The five year cycles could be detected only in one of the precipitation time series included in the catchment average time series. This different periodic behaviour is likely caused by different geographical and climate conditions in the Danube Basin. Furthermore, catchment average precipitation time series were used instead of time series measured at a single climatic station in the above indicated studies. The global wavelet spectrum test of the climatic stations found long cycles in precipitation in the north eastern and south western segments of the analysed geographical area. These segments approximately correspond to the climatological regionalization according to (Auer et al., 2007).

Similarly to (Markovic and Koch, 2013), no significant long cycles were found in the mean monthly temperature time series. This, however, differs from the findings of (Andreo et al., 2006), who were able to detect long cycles in temperature. This may be attributed to the different climatic conditions - unlike in the upper Danube region, the temperatures on the Iberian peninsula analysed by (Andreo et al., 2006) are strongly influenced by the Atlantic ocean and Mediterranean sea.

Long range dependence was found in all discharge time series. The presence of long range dependence in the Danube River discharges is in accordance with findings of Mudelsee (2007), Szolgayova et al. (2013). Despite the fact that no long cycles could be detected in the temperature time series, all of these display long term persistence. Thus the long range dependence is likely driven by some other non - cyclical mechanism or process. No long range dependence could be found in monthly precipitation time series. This might indicate, that even though long cycles in precipitation do influence the Hurst coefficient of discharge, there are other significant factors, such as catchment storage characteristics, as suggested by (Szolgayova et al., 2013).

The wavelet spectra of each of the observed time series were analysed as well. The high correlation between the respective time series contributes to the high degree of similarity between the spectra for each variable. In addition, the similarity between the temperature spectra is caused by the method of calculation of these time series. A visual decrease in the significant low frequency parts of the spectrum in the precipitation time series can be observed as we move downstream. This was accompanied by the decrease of the respective Hurst coefficients. Significant low frequency spots in the temperature spectra were observed for the years with daily temperature minima over years below the long time temperature average.

The relationships between precipitation, temperature and discharge time series were analysed using the cross - wavelet spectra and wavelet coherence. The precipitation - discharge wavelet coherence spectrum showed significant coherence for most of the periods at almost all time as would be expected. This is in agreement with the high consistency of precipitation and discharge decadal variability in the Danube basin found by (Rimbu et al., 2002). The non - significant part of the wavelet coherence spectrum between precipitation and discharge ending in the early in the 1960s corresponds to the period, where almost no significant floods occurred on the Danube River (Blöschl and Montanari, 2010). This may be due to a regime switch in the precipitation time series.

A finding that is considered particularly interesting is the lead time between precipitation and discharge found from the cross wavelet spectra. At the period of four years, precipitation leads discharge by about six months. Soil moisture storage and near-surface groundwater have typical residence times of this order of magnitude. Interestingly, for

the longer period of 11-14 years, the lead time is also longer (around 3 years). This suggests that deeper groundwater storage is accessed when long-term decadal fluctuations in precipitation and discharge occur which is not the case of the shorter term fluctuations. This can be clearly seen in Fig.4.7 where a constant time lag has been used for generating discharge for all periods and consequently the lead time does not increase with the period. The effect of deeper groundwater storage is accessed is likely related to the non-linearity of the rainfall-runoff transformation which has been documented in numerous catchments around the world (eg. (Wittenberg, 1999)). Furthermore, in the 1960s, the phase difference in the period of four years tends to decrease from six to one to two months. It is possible that this is also related to storage effects where shallower aquifers are accessed due to changes in the water balance.

A discharge convolution function was constructed in order to gain better understanding of the information provided by the wavelet spectra and the long range dependence in precipitation. The periodic behaviour of the discharge time series was acceptably reproduced using the convolution. The convolution results indicate that the long range dependence in discharge is partly influenced by the long range dependence in precipitation and partly by the non-linear catchment storage processes. It can be seen that the lead time of precipitation increases with the increasing weight of the long time kernel representing the rainfall-runoff relationship. This kind of convolution function could be used as a basis for a more sophisticated rainfall runoff wavelet based model, attempting to include and reproduce the phase shifts between the time series found in the cross-wavelet spectra (Kwon et al., 2007, Renaud et al., 2003).

The results show that especially mean monthly precipitation could be used in multivariate stochastic discharge time series modelling when considering a monthly time step, for example by means of a wavelet based model using wavelet decomposition and wavelet coherence in order to obtain a multivariate stochastic discharge model. Furthermore, additional wavelet analysis can be conducted in combination with other climate phenomena, such as the North Atlantic Oscillation in order to attribute the cycles found especially in precipitation and thus explain the found cyclical behaviour of the precipitation and temperature time series on larger scale. The findings of this paper give insights into the cyclical behaviour and changes of such behaviour of monthly discharge of the Danube river in central Europe and how these changes are influenced by precipitation and temperature in the respective catchment areas.

Chapter 5

Wavelet based deseasonalization for modelling and forecasting of daily discharge series considering long range dependence

Abstract

Short term streamflow forecasting is important for operational control and risk management in hydrology. Despite a wide range of models available, the impact of long range dependence is often neglected when considering short term forecasting. In this paper, the forecasting performance of a new model combining a long range dependent autoregressive fractionally integrated moving average (ARFIMA) model with a wavelet transform used as a method of deseasonalization is examined. It is analysed, whether applying wavelets in order to model the seasonal component in a hydrological time series is an alternative to moving average deseasonalization in combination with an ARFIMA model. The one to ten days ahead forecasting performance of this model is compared with two other models, an ARFIMA model with moving average deseasonalization and a multiresolution wavelet based model. All models are applied to a time series of mean daily discharge exhibiting long range dependence. For one and two day forecasting horizons, the combined wavelet - ARFIMA approach shows a similar performance as the other models tested. However, for longer forecasting horizons, the wavelet deseasonalization - ARFIMA combination outperforms the other two models. The results show that the wavelets provide an attractive alternative to the moving average deseasonalization.

5.1 Introduction

Short term forecasting is important in operational hydrology for reservoir operations and risk control (McLeod and Hipel, 1994). There are several approaches for short term modelling and forecasting, including deterministic conceptual rainfall-runoff models Blöschl and Montanari (2010), Reszler et al. (2008) and a wide range of stochastic models, such as autoregressive (Burlando et al., 1993, Quimpo, 1969) or regime switching models (Ko-

morník et al., 2006, Komorníková et al., 2008) or neural networks (C.M. Zealand and Simonovic, 1999, Maier and Dandy, 2000).

Removing systematic components (trend and seasonality) in the process of time series modelling is therefore part of the standard time series modelling paradigm (Box and Jenkins, 1976). The seasonality of streamflows stems from the earth rotation and can be explained by the physical processes in the catchment, such as snowmelt and precipitation. Therefore it is often removed in stochastic streamflow modelling (Komorník et al., 2006, Komorníková et al., 2008, Prass et al., 2012). Thus deseasonalization simplifies time series modelling and forecasting and possibly widens the model choice. There are numerous studies elaborating on the stochastic part of the model (for example see (Koop et al., 1997, Montanari et al., 1997, Ooms and Franses, 2001)), however studies focusing on deseasonalization are lacking.

Despite the huge range of models available, the impact of long range dependence is often neglected when considering short term forecasting. However, (Prass et al., 2012) found, that long range dependence may have an impact on the performance of short term modelling. Long term dependent processes are characterized by hyperbolic decrease of the autocorrelation function and are closely related to self-similarity (Doukhan et al., 2003). Long range dependence has been encountered in various hydrological (Ehsanzadeh and Adamowski, 2010, Koscielny-Bunde et al., 2006, Lye and Y.Lin, 1994, Pelletier and Turcotte, 1997) and other data. Incorporating long range dependence into time series modelling is important, since the model should capture the behaviour of the data as realistically as possible. Autoregressive fractionally integrated moving average (ARFIMA, (Beran, 1994)) models are a tool often used for the modelling of long range dependent time series ((M. Lohre and Könnig, 2003, Montanari et al., 1997, Prass et al., 2012)).

The presence of periodic or seasonal components generally has an effect on long range dependence estimation (Montanari et al., 1999b). However, the possibility of improving the deseasonalization step is scarcely discussed, even though each deseasonalization method has an effect on the covariance structure of the resulting time series, thus influencing the Hurst coefficient and the following model parameters.

Wavelet decomposition is a popular tool used to model and forecast (Renaud et al., 2003, Starck et al., 1998) periodic behaviour of time series. In hydrology, wavelets are scarcely used for forecasting (Adamowski, 2008) and wavelet modelling in hydrology is done especially in combination with neural networks (Renaud et al., 2003, S. Wei and Khan, 2012, Thuillard, 2002, Yousefi et al., 2005). In general, more attention is paid to feature extraction and detailed process description (Andreo et al., 2006, Grinsted et al., 2004, Pasquini and Depetris, 2010, Torrence and Compo, 1999) rather than to their potential to be employed for deseasonalization.

Since wavelets are able to capture the changes in a given frequency interval over time, they thus make it possible to describe the changes in the annual cycle of the discharge time series as a reaction to its driving processes, such as precipitation. It seems this would be a more process based approach to the deseasonalization of the discharge time series than the moving averages deseasonalization method. The main objective of this study is to therefore to examine, whether applying wavelets in order to model the seasonal component in a hydrological time series is an alternative to moving average deseasonalization in combination with a long - range dependent ARFIMA model. To examine the potential of the approach for practical applications, three models will be compared through their

actual one to ten steps ahead forecasting performance. The following questions will be analyzed: What are the effects of deseasonalization on the model fit and forecasting performance in a daily discharge time series with long range dependence? How is the model prediction performance affected by the alternative deseasonalization procedure? Is wavelet decomposition a suitable method for removing the seasonal component of daily discharge series?

In order to address these questions we adjust the standard modelling concept (Box and Jenkins, 1976) by replacing the generally used moving average seasonal filter by a wavelet filter, thus obtaining a combined wavelet - ARFIMA model. This will be applied to a series of daily river discharges from Lower Austria and 1 to 10 - steps - ahead forecasts will be compared with a classical model combining the removal of seasonal components via moving averages smoothing and an ARFIMA model and a purely wavelet based model.

5.2 Methods

In order to assess the impact of removing the seasonal components from a time series on model fit and forecasting, three different models will be considered. An overview can be seen on Figure 5.1.

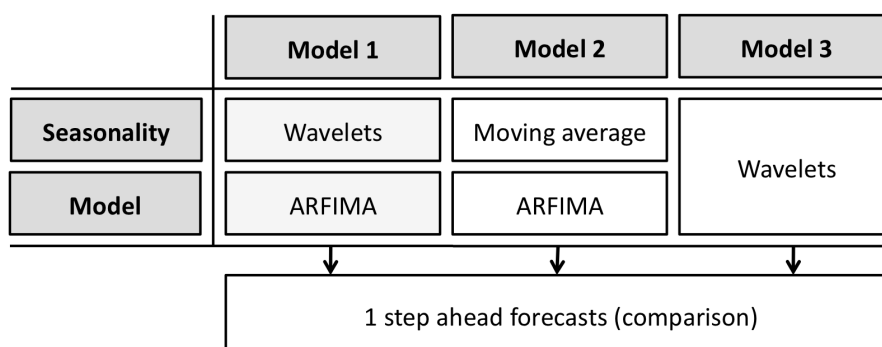


Figure 5.1: Analysis overview

The first model uses a suitable frequency interval to remove the most significant seasonal components by wavelet decomposition and fits an ARFIMA model to the residuals. In the second model, the standard approach combining a moving average deseasonalization with an ARFIMA model is applied. The last approach is based on wavelet decomposition and a multiresolution model according to Renaud et al. (2003). All the three models are described in detail later in this section. In general, the modelling procedure for the first two models is as follows:

1. Removing trend and seasonality
2. Fitting of the $ARFIMA(p, d, q)$ model
3. 1 to 10 -steps-ahead forecasts construction

In the last model, steps 1 and 2 are replaced by a wavelet decomposition and a multiresolution model fit.

5.2.1 Description of the models

Model one

The maximum overlap discrete wavelet transform (MODWT) Gencay et al. (2001) with the least asymmetric wavelet of order eight is applied for modelling the seasonal component in model one. This wavelet can not be given in a closed form and the coefficients are calculated iteratively. For details see Daubechies (1992).

The forecasts $X_{T+s+1}, \dots, X_{T+s+h}$, $s = 0, \dots$ for the observed time series X_1, \dots, X_{T+s} are calculated in following steps

- A wavelet transform of the time series X_{s+1}, \dots, X_{T+s} is performed. Starting at X_{s+1} implies, that the length of the transformed time series is always constant, thus the annual periodicity is being maintained at each time step. In general, a disadvantage of the MODWT algorithm is the presence of edge effects due to the circular shift of the time series, possibly causing significant inconsistencies in the forecasted seasonal component. The loss of information caused by leaving out observations from the beginning of the time is not significant due to the overall length of the modelled dataset (over 9000 observations).
- A trigonometric function to the wavelet coefficients is fitted, followed by the inverse transform in order to obtain the forecasts of the seasonal component Yousefi et al. (2005). A two stage linear least squares fit Dou and Chan (1998) is used to estimate the trigonometric function. In the first step a linear problem is solved, where the phase shift and amplitude of a sinusoidal function are fitted, in the second step the frequency of the signal is estimated by

$$\min_{\omega} \{ \min_{A, \theta} J_{\omega}(A, \theta) \} \quad (5.1)$$

where $J_{\omega}(A, \theta) = \sum_{t=0}^{T+s} (X_t - A \sin(\omega t + \theta))^2$, A is the amplitude, ω the frequency and θ the phase shift of the signal.

- The time series is deseasonalized. The h - step - ahead forecast from the deseasonalized time series using the ARFIMA model is calculated.
- The forecast of the seasonal component obtained as indicated in previous steps is then added to the ARFIMA forecast in order to obtain the overall model forecast for the days $X_{T+s+1}, \dots, X_{T+s+h}$.

In model one, forecasting from the resolution level containing the annual periodicity of the detail signal $D_{j,t}$ is needed. On the other hand in model three (described later), $D_{j,t}, S_{j,t}$ for all $j = 1 \dots J$ are necessary for a forecast calculation. For this reason, two different methods are applied in the data analysis.

Model two

Model two is constructed analogically to model one, using the moving average deseasonalization method described in section 2.3.

The forecasts $X_{T+s+1}, \dots, X_{T+s+h}$ are calculated as follows

- The seasonal filter is recalculated including the newly obtained observation X_{T+s} . The seasonal forecast is then $F_{((T+s+1) \bmod 365)}, \dots, F_{((T+s+h) \bmod 365)}$.
- X_1, \dots, X_{T+s} is deseasonalized using the updated seasonal filter.
- The ARFIMA forecast is calculated.
- The overall forecast is calculated by adding the ARFIMA forecast and the forecast of the seasonal component.

Model three

In the model three the non-decimated Haar à trous algorithm is used Shensa (1992). Applying a convolution filter $h = (0.5, 0.5)$ yields

$$s_{j+1,t} = \frac{1}{2}(s_{j,t-2^j} + s_{j,t}) \quad (5.2)$$

$$d_{j+1,t} = s_{j,t} - s_{j+1,t} \quad (5.3)$$

From equations (5.2), (5.3) can be seen, that the end of the signal is not being shifted during the wavelet transform, thus the already calculated wavelet coefficients remain unchanged, when new observations X_{T+1}, X_{T+2}, \dots are included into the transform Renaud et al. (2003). This makes this methods especially suitable for forecasts, since the edge effects due to the usually performed circular shift of the time series applied during the wavelet transform do not occur.

In this particular case $X_t = s_{J,t} + \sum_{j=1}^J d_{j,t}$ holds, thus the wavelet coefficients are used directly to construct the forecasts. A linear multiscale autoregressive concept suggested in Renaud et al. (2003) is used for the forecasting (model three):

$$\hat{X}_{T+1} = \sum_{j=1}^J \sum_{k=1}^{A_j} a_{j,k} d_{j,T-2^j(k-1)} + \sum_{k=1}^{A_{J+1}} a_{J+1,k} s_{J,T-2^J(k-1)} \quad (5.4)$$

where A_j are the orders of the autoregressive model for each frequency interval. In this chapter $A_j = 2$ was used for all resolution levels.

5.2.2 Forecasts comparison

The forecasting performance is evaluated using the modified Diebold Mariano test Diebold and Mariano (1995), Harvey et al. (1997), the Nash-Sutcliffe coefficient Nash and Sutcliffe (1970) and the Theil's inequality coefficient Theil (1958). The model outputs are furthermore visually compared using scatter plots of measured and forecasted runoffs.

Consider two competing models A and B . The modified Diebold Mariano test tests the null hypothesis H_0 : A, B produce equally accurate h -steps-ahead forecasts. The test statistics is given by

$$MDM = \left(\frac{m+1-2h+h(h-1)/m}{m} \right)^{1/2} \frac{\bar{d}}{(mV(\bar{d}))^{1/2}} \quad (5.5)$$

where m is the length of the interval, on which the (out-of sample) h -steps-ahead forecasts are made (h is the forecasting horizon) and $\bar{d} = \frac{1}{m+1} \sum_{s=0}^m d_s = \frac{1}{m+1} \sum_{s=0}^m (\hat{e}_{T+s}^A(h) - \hat{e}_{T+s}^B(h))^2$. Here $\hat{e}_{T+s}^A(h) = \hat{X}_{T+s}^A(h) - X_{T+s+h}$ are the model errors, forecasts being denoted as $\hat{X}_{T+s}^A(h)$ for $s = 0, \dots, m$ (i.e. $\hat{X}_{T+s}^A(h)$ is the forecasted runoff for the day $T + s + h$ with h days forecasting horizon and the forecasting threshold $T + s$). $V(\bar{d})$ is the estimate of the variance of d_s . The test output has three possible entry values: 0 (statistically equivalent performance), -1 or 1 representing significantly worse or better performance of model A compared to B respectively.

The Nash-Sutcliffe coefficient E is widely used in hydrology to assess the forecasting performance (K.Jain and Sudheer (2012), Nash and Sutcliffe (1970)) and it is defined as

$$E = 1 - \frac{\sum_{s=0}^m \hat{e}_{T+s}^2(h)}{\sum_{s=0}^m (X_{T+s+h} - \bar{X})^2} \quad (5.6)$$

where $\bar{X} = \frac{1}{T} \sum_{t=1}^T X_t$. In general $E \in (-\infty, 1]$, higher values indicating better performance, $E = 1$ meaning a perfect forecast.

The Theil inequality coefficient U is defined as

$$U = \frac{\sqrt{\frac{1}{m+1} \sum_{s=0}^m \hat{e}_{T+s}^2(h)}}{\sqrt{\frac{1}{m+1} \sum_{s=0}^m \hat{X}_{T+s}^2(h) + \sqrt{\frac{1}{m+1} \sum_{s=0}^m X_{T+s+h}^2}}} \quad (5.7)$$

For the Theil coefficient holds $U \in [0, 1]$, the quality of the forecast increasing with the decreasing U .

5.3 Results

The described models are applied to a time series of mean daily runoffs of the Danube River at the gauge Kienstock near the city of Krems an der Donau in Lower Austria. The catchment area corresponding to the Kienstock gauge is 95970 km^2 .

The time series displays periodic behaviour due to the seasonal components in the weather over the year typical of the continental climate. No trend was found in the time series. The three models were fitted for the period January 1982 - December 2006 and verified for the consecutive two years.

Figure 5.2 shows the series of daily mean runoffs from the Kienstock gauge used in the analyses and the periodogram of the data. The highest peak in the periodogram represents the annual periodicity in the time series.

Since discharge takes only positive values, the natural logarithm of the original series was used in the analysis (let us denote $X'_t = \ln X_t$). M. Lohre and Könnig (2003) (thus the forecast was obtained as $\hat{X}_{T+s}(h) = \exp(\hat{X}'_{T+s}(h))$). This transformation also brings the distribution of the data closer to the normal distribution, which is assumed by the ARFIMA model.

5.3.1 Model fit

For the wavelet deseasonalized series (model 1), the sub-series $D_{8,t}$ was subtracted from the series X'_t . $D_{8,t}$ corresponds to the frequency interval $(2^{-9}, 2^{-8})$, which includes the

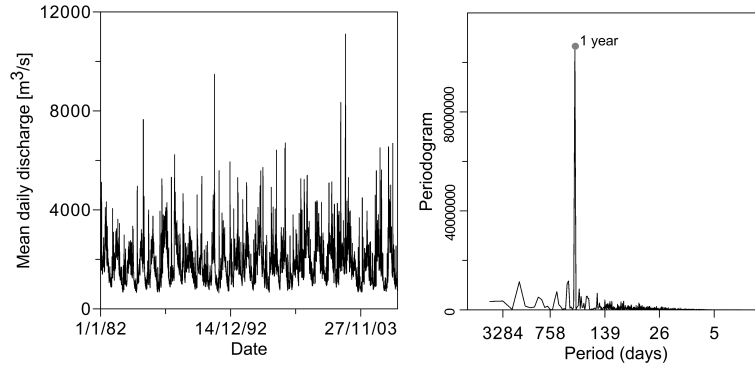


Figure 5.2: Danube daily discharge at the Kienstock gauge, period 1.1.1992 - 31.12.2006 (left) and the periodogram of the time series (right)

annual periodicity of 365 days. A comparison of the seasonal components removed by subtracting $D_{8,t}$ (wavelet deseasonalization) and the smoothed daily averages (moving average deseasonalization) can be seen of Figure 5.3. The resulting seasonal filters are rather similar for both methods. This is expected, since the seasonal behaviour of the discharge process is assumed to be similar every year. However it can be seen, that unlike the MA filter, the wavelet filter is changing over the years, thus reacting to changes in the driving processes in the catchment. The wavelet spectrum of the time series for the corresponding time period is depicted under the deseasonalization filters. This explains the irregularities in the wavelet deseasonalization method (for example in the year 2002), where the annual frequency is not so significant as in the rest of the time series. The wavelet spectrum and the wavelet deseasonalization thus reflect the actual behaviour of the runoff in that periods - the floods in august 2002 (counting among the most significant of 20th century Pekárová et al. (2013)) and the drought in the year 1997 Patassiová et al. (2002). Unlike the wavelet deseasonalization, the moving average deseasonalization does not capture such irregular changes in the seasonal components which might be present in the time series.

The change in the ACF of the time series after removing the seasonal components is shown on Figure 5.4. A difference in the two deseasonalization approaches is especially visible from the periodogram figures. The wavelet deseasonalization is more "thorough" - the frequency band around the annual periodicity of 365 days is mostly filtered out. A closer observation of the ACFs at the lags around one year shows however, that the moving average deseasonalization was able to remove the autocorrelation better than the wavelet method for this particular area.

For the ARFIMA models various p, q combinations were fitted, based on the ACF and the partial autocorrelation function. These models were compared using the Akaike information criterion. In both cases, an ARFIMA(1,d,1) model was chosen as the most suitable one. The model parameters are shown in Table 5.1. The difference in the constant term c occurs since the moving average deseasonalization centers the time series, but the wavelet component has zero mean, and thus has no impact on the time series from this point of view and has to be removed later in the modelling process.

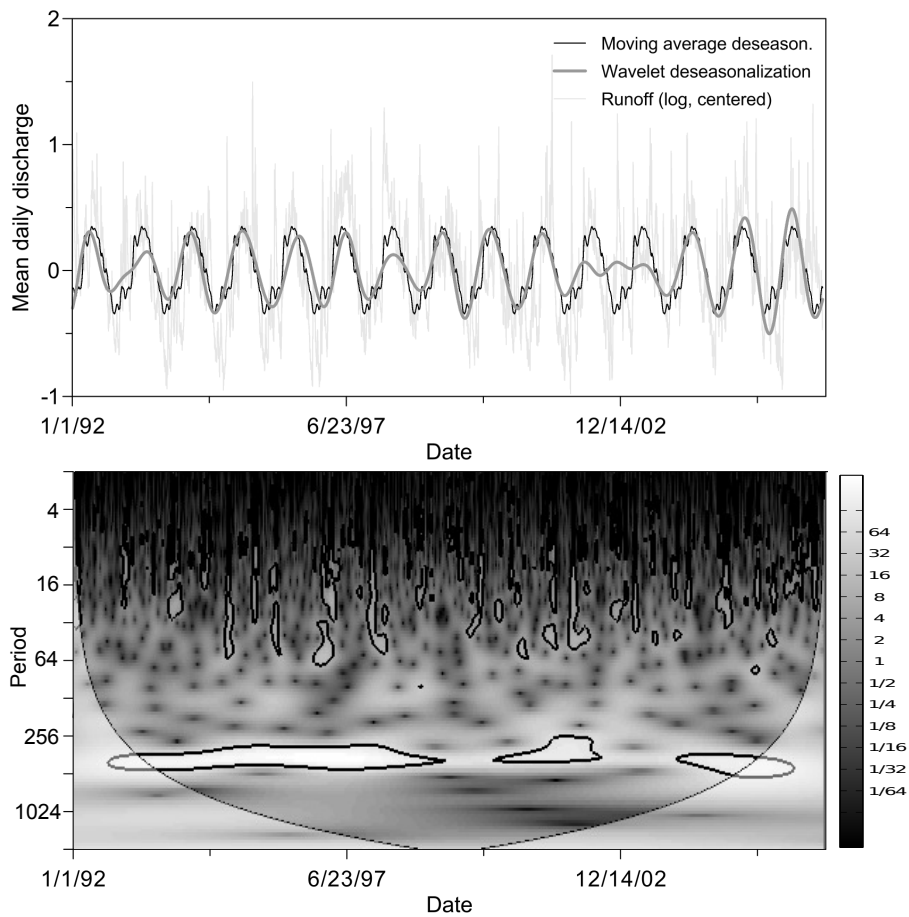


Figure 5.3: The image on the top shows the series used for deseasonalization; the moving average of daily means and the wavelet filter, both for the period 1992-2006. The bottom image is the wavelet spectrum of the time series for the corresponding period. The white band in the lower part of the figure corresponds to the annual periodicity, as indicated on the vertical axis of the figure.

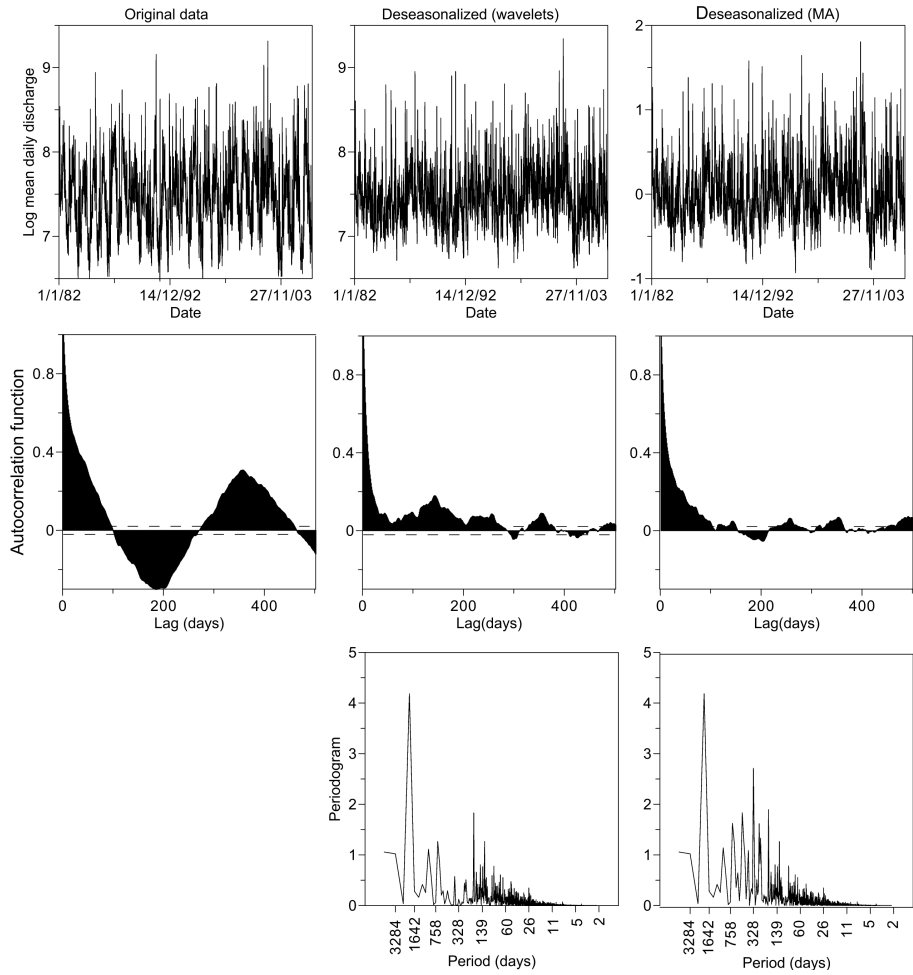


Figure 5.4: Autocorrelation function of the time series. The left pictures show the (logarithm) of the original runoff time series and its autocorrelation function. The figures on the right depict the autocorrelation function after deseasonalization (using wavelets in the middle and using the moving average subtraction on the right) and the respective residual series. In the bottom of the Figure there are the periodograms calculated after the application of the respective deseasonalization method.

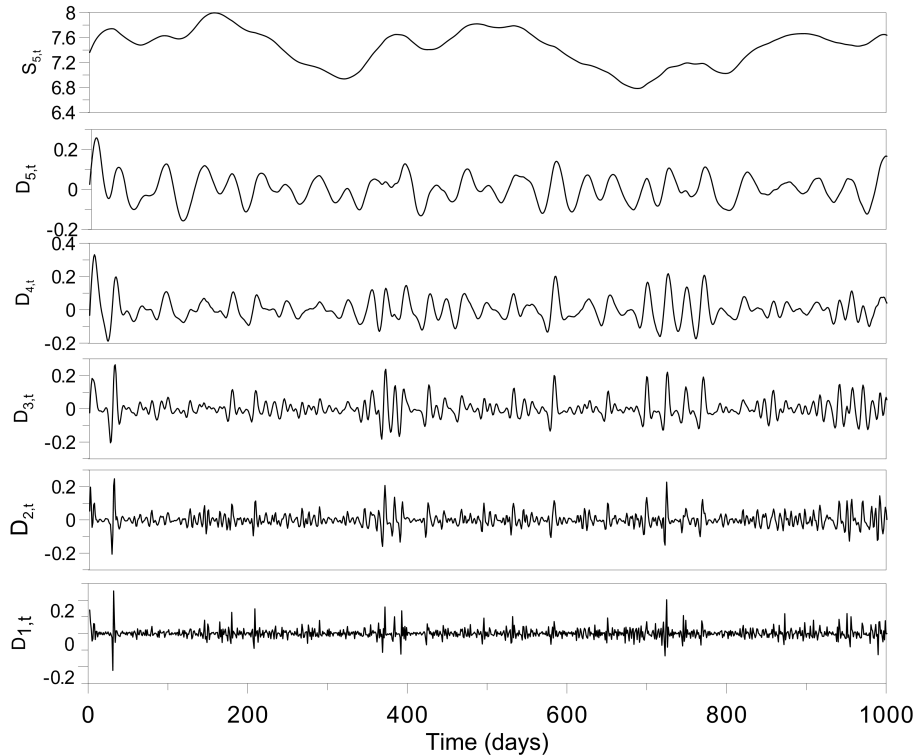


Figure 5.5: The smooth and detail time series components calculated using the (inverse) Haar wavelet transform (model 3)

Model	d	ϕ_1	θ_1	c
1	0.26	0.73	0.28	7.44
2	0.33	0.68	0.25	0

Table 5.1: Parameters of the fitted ARFIMA models (equation 2.30)

The Hurst coefficient estimates following from the model fit are derived from the respective differencing parameters of the model, obtaining $H_{\text{model 1}} = 0.76$ and $H_{\text{model 2}} = 0.83$. Since both estimates are higher than 0.5, the respective processes display long range dependence, justifying the choice of the ARFIMA model.

An inverse wavelet transform of the log daily discharges using the Haar wavelet can be seen on Figure 5.5. For model 3 both $J = 5$ and $J = 10$ models were constructed, their forecasting performance was equivalent, thus the simpler model was chosen for the final comparison.

The autocorrelation functions of the residuals of all three models are on Figure 5.6. In each case, the models are able to remove almost all significant autocorrelation structure.

5.3.2 Forecasting comparison

Based on the fitted models 1 to 10 days ahead forecasts were constructed for the two years (730 days) following the fitting period.

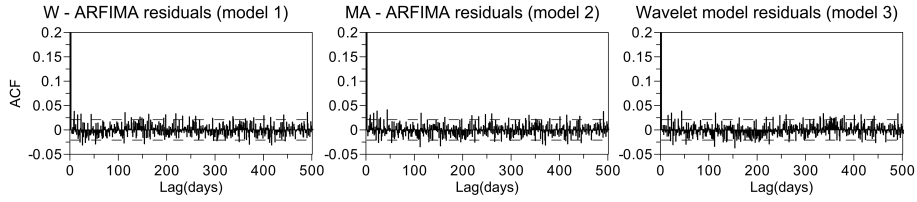


Figure 5.6: Autocorrelation function of the residuals for each of the three applied models. The dashed lines depict the significance bounds.

The comparison of the forecasting performance for all considered forecast horizons is in Table 5.2. In general, for a fixed horizon h the forecasts are of comparable quality when comparing the Theil's coefficient and Nash - Sutcliffe coefficients, especially for $h < 4$. For 1 and 2 steps ahead forecasts all the three models deliver statistically equivalent forecasts as can be seen from the results of the modified Diebold - Mariano test. However, the forecasting performance changes with the increase of the forecasting horizon. For $h = \{3, \dots, 5\}$ the wavelet - ARFIMA (model 1) outperforms the MA - ARFIMA model (model 2) and for higher forecasting horizons the wavelet model (model 3) as well. Furthermore for $h = 10$ the wavelet model performs worse than the other two considered models. As can be seen from the Nash - Sutcliffe coefficient E , with increasing forecasting horizon, the deterioration of the quality of the forecasts of the multiresolution wavelet model (model 3) is faster compared to the other 2 models for $h > 5$. For $h = 10$ we have $E_{m,3} = 0.03$ which indicates forecasting with the mean of the time series is almost equivalent as the wavelet forecast. For the other two models we have $E_{m,1} = 0.12$ and $E_{m,2} = 0.07$. However, the forecasting performance is decreasing dramatically with the increase of the forecasting horizon (compare the Nash - Sutcliffe and Theil coefficients in Table 5.2) for all three models, which is not unexpected.

Both the Nash-Sutcliffe coefficient (for all models approximately 0.84) and the Theil's inequality coefficient (approximately 0.07 in all cases) indicate good forecasting performance for one - day - ahead forecasting horizon.

Scatter plots of observed versus predicted runoffs for $h = \{1, 3, 6, 10\}$ can be seen on Figure 5.7. These particular horizons were chosen since here the comparative forecasting performance of the respective models changes (see the MDM test in Table 5.2). The deterioration of the forecasting quality can be seen from the scatterplots. All scatter plots indicate a problem of the respective model, when extreme runoff values (i.e. potential floods) appear in the time series.

5.4 Discussion and conclusions

The main objective of this study was to examine, whether applying wavelets in order to model the seasonal component in a hydrological time series is an alternative to moving average deseasonalization in combination with a long - range dependent ARFIMA model. A comparison of the forecasting performance in term of 1 to 10 steps ahead forecasts of these two models was conducted. An additional comparison with a simple linear purely wavelet based model was provided. The models were applied to a time series of daily mean discharge of the River Danube, measured at gauge Krems.

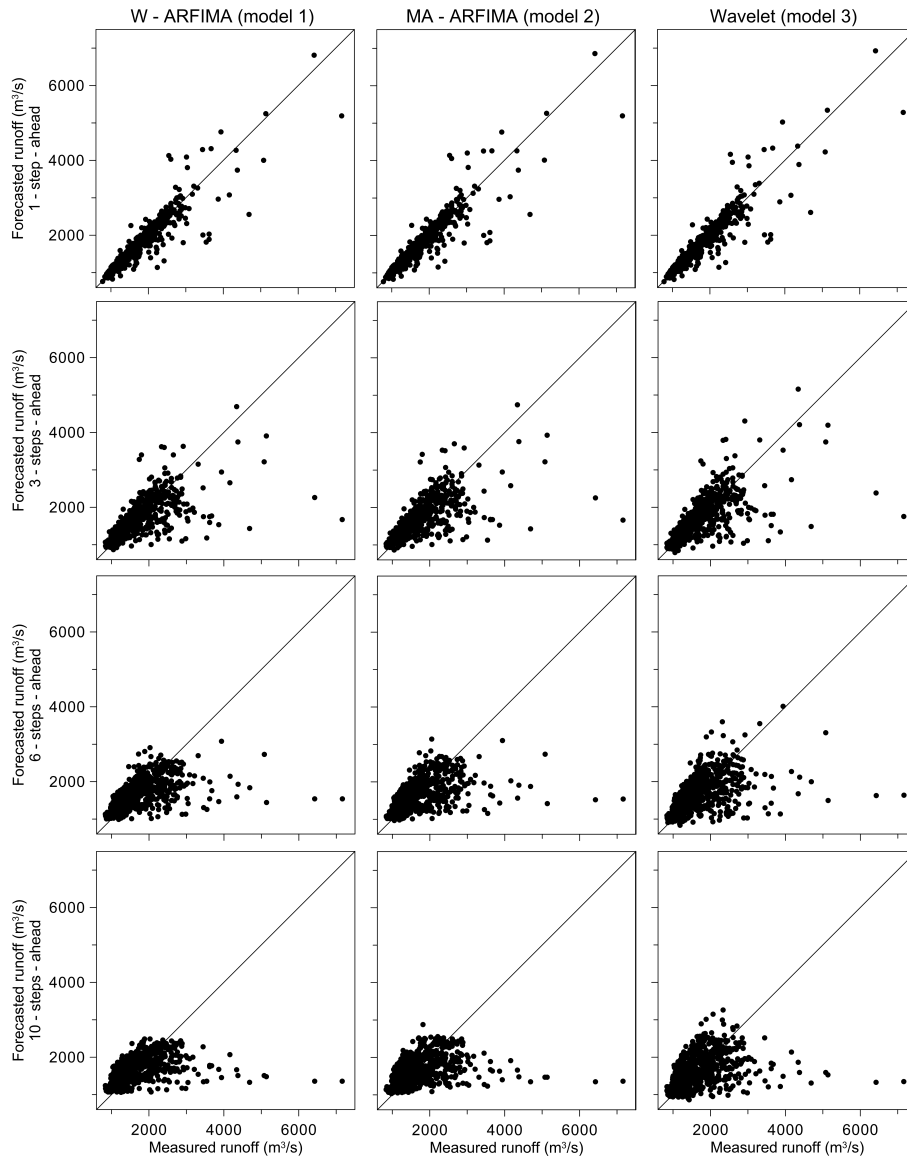


Figure 5.7: Scatterplots of measured daily discharges versus the forecasted discharges using all three models. Forecasting horizons of 1, 3, 6 and 10 days are shown.

	Forecasting horizon									
	1	2	3	4	5	6	7	8	9	10
W - ARFIMA										
<i>E</i>	0.84	0.60	0.43	0.33	0.27	0.23	0.20	0.17	0.14	0.12
<i>U</i>	0.07	0.12	0.14	0.15	0.16	0.16	0.17	0.17	0.17	0.18
<i>MDM</i> (<i>m. 2</i>)	0	0	1	1	1	1	1	1	1	1
<i>MDM</i> (<i>m. 3</i>)	0	0	0	0	0	1	1	1	1	1
MA - ARFIMA										
<i>E</i>	0.84	0.60	0.42	0.31	0.24	0.2	0.17	0.13	0.1	0.07
<i>U</i>	0.07	0.12	0.14	0.15	0.16	0.17	0.17	0.17	0.18	0.18
<i>MDM</i> (<i>m. 1</i>)	0	0	-1	-1	-1	-1	-1	-1	-1	-1
<i>MDM</i> (<i>m. 3</i>)	0	0	0	0	0	0	0	0	0	1
Wavelets										
<i>E</i>	0.84	0.6	0.42	0.31	0.24	0.19	0.15	0.11	0.06	0.03
<i>U</i>	0.07	0.12	0.14	0.15	0.16	0.17	0.17	0.18	0.18	0.18
<i>MDM</i> (<i>m. 1</i>)	0	0	0	0	0	-1	-1	-1	-1	-1
<i>MDM</i> (<i>m. 2</i>)	0	0	0	0	0	0	0	0	0	-1

Table 5.2: Forecasting performance comparison - outputs from the Nash - Sutcliffe coefficient (*E*) and the Theil's coefficient (*U*) and the modified Diebold Mariano test (*MDM*). For the *MDM* test, the comparison model is given in parentheses.

It would seem plausible, that wavelets, since localized both in time and frequency, thus able to capture the irregularities in the seasonal cycle better than the traditional moving average method, would provide an improvement to the traditional model. Unlike the rather generic moving average filter, which reflects the average behaviour of the time series on a daily basis, the wavelet deseasonalization is based on a more detailed description of the time series in the respective frequency interval, thus more reflecting on the physical behavior of the discharge. Indeed, the wavelet deseasonalization was able to capture atypical behaviour, such as the floods in the year 2002.

Both of the models using the two different deseasonalization methods delivered statistically equivalent forecasts for one and two days ahead forecasts. The fact, that the wavelet - ARFIMA model did not outperform the other model for $h = 1, 2$ may be due to several reasons. Firstly, the wavelet transform (repeated in each day of the forecasting period) suffers from edge effects Torrence and Compo (1999). This has a negative impact on the forecasting performance. Secondly, a trigonometric function was fitted to the wavelet coefficients in order to model the seasonal component. The trigonometric function is periodic, thus the ability of the wavelets to capture the temporal irregularities could not be exploited in full. This effect was however dampened by the use of the inverse transform following the trigonometric fit. The good comparable performance of an autoregressive model compared to an ARFIMA model, even in case of long range dependence was pointed out already by Crato and Ray (1998).

The linear wavelet based model performed well (as indicated by both Nash - Sutcliffe and Theil coefficient) for short forecasting horizon, which is in general accordance with

the literature Renaud et al. (2003). The quicker deterioration of the wavelet based model compared with the other two ARFIMA models might indicate, that incorporating long range dependence even if considering daily time steps could be profitable. Similarly, Prass et al. (2012) showed improvement in short term forecasting when incorporating long range dependence into a model on data with monthly time step.

For longer forecasting horizons ($h > 2$) the combined wavelet - ARFIMA model outperformed the other two models. The quality of the forecasts decreased significantly with the increase of the forecasting horizons for all three models, however this was especially pronounced in the case of the linear wavelet model for $h > 5$. This is in accordance with general properties of time series forecasting Brockwell and Davis (2002). It can be concluded, that for longer forecasting horizons, the quality of the forecasts of the new wavelet - ARFIMA model is statistically better than the traditional combination of moving average deseasonalization with ARFIMA. For higher forecasting horizons the wavelet - ARFIMA model outperforms the multiresolution wavelet model as well (according to the Diebold Mariano test). Thus the wavelet deseasonalization offers improvement in time series forecasting for time series with long range dependence for higher forecasting horizons.

Finally, it should be noted, than none of the three models was able to remove autocorrelation from the squared residuals after the model fit. This autocorrelation usually indicates heteroscedasticity in the time series, thus the concept of the wavelet deseasonalization may be explored further in combination of other possibly suitable model, such as a fractionally integrated generalized autoregressive conditional heteroscedasticity Ehsanzadeh and Adamowski (1982), Modarres and Ouarda (2012) model type.

Chapter 6

Summary of results and conclusions

The aim of this thesis was to analyse discharge and some of its driving processes from a long term perspective, in order to be able to improve stochastic time series modelling in the future. In order to achieve this goal, long range dependence and long cycles in discharge time series were analysed. Correlations with various external drivers were calculated and finally these findings were incorporated into the classical time series modelling concept using a model considering long range dependence.

Chapter 3 analyses the correlations between the long range dependence measured by the Hurst coefficient and various climate and storage related catchment attributes in 39 annual discharge time series of European rivers. Long range dependence was found in all time series. The estimates obtained from the different estimation methods used in this chapter were consistent. Correlations between the Hurst coefficients and various catchment attributes were calculated. No significant correlation was found between long range dependence, elevation and time series length. Positive dependence was found for mean discharge, catchment area and mean annual air temperature. Negative correlation was found for annual precipitation for some of the estimation methods. The results of the correlation analysis can be related to catchment area effects, catchment wetness, and snow processes.

In Chapter 4 continuous wavelet analysis was applied in order to analyse the long term behaviour of (monthly) discharges of the Danube River and their relationship to long term behaviour in air temperature and precipitation. Several long cycles were identified in the analysed time series, some with periodicities of more than a decade. An 11 -13 years cycle was detected in precipitation. The periodic behaviour of the precipitation time series varied based on the station analysed, probably influenced by different geographical conditions. No significant cycles were found in the air temperature series. The cross - wavelet spectra of discharge and each of the other time series were analysed as well. The precipitation - discharge wavelet coherence spectrum showed significant coherence for most of the periods almost all the time. The non - significant part of the wavelet coherence spectrum corresponds to the period, where almost no significant floods occurred on the Danube River. The various lead times found in the cross - wavelet spectra were interpreted in terms of soil moisture and groundwater storage.

Chapter 5 used discrete wavelet transform for modelling of the seasonal component of a discharge time series with long range dependence in combination with an ARFIMA model. A comparison with the standard approach was offered via forecasting perfor-

mance. The wavelet deseasonalisation model was able to capture the seasonal anomalies more accurately than the generic moving average mean deseasonalisation method. For short forecasting horizons, the two methods did not show any significant differences in the forecasting performance. However, with the increase of the forecasting horizon, the wavelet deseasonalization method outperformed the standard model setup. Unfortunately, neither of the approaches was able to remove conditional heteroscedasticity from the time series, leaving space for further modelling improvements.

Based on the findings of the thesis further interesting issues which should be investigated in the future, emerge. Obviously, the discharge time series modelling is rather complex, being influenced by many other variables and processes. These are usually taken into consideration in the conceptual models, however multivariate stochastic discharge models are lacking. Even though the univariate approach usually produces reasonable model fit and acceptable quality of simulated time series, such models do not react to general change in the underlying processes, such as an increase in average air temperature and precipitation in the catchment. Thus in the future, construction of multivariate discharge models would be desirable. Air temperature, precipitation or from the derived variables, such as the antecedent precipitation index can be used as external explanatory variables. Results of Chapter 5 show, that heteroscedasticity is possibly present in discharge time series. Furthermore, the wavelet spectra investigated in Chapter 4 indicate, there might be switches in the regimes of the data, especially in the precipitation series. Thus regime switching models or a heteroscedastic autoregressive model would be a reasonable start for such modelling. Furthermore, long range dependence should be considered. Such models could be used for construction of long simulated discharge series, analysing the impact of changes in the climate in terms of precipitation and air temperature on discharge.

The results of this thesis have important implications for stochastic hydrological modelling especially for water resources management and reservoir operation. They emphasize the need for case based model construction under consideration of long range dependence or other long term phenomena present in the time series. Furthermore, they emphasize the need for multivariate discharge models, incorporating the dependencies between discharge, precipitation and air temperature into stochastic time series models.

Bibliography

- J.F. Adamowski. Development of a short-term river flood forecasting method for snowmelt driven floods based on wavelet and cross-wavelet analysis. *Journal of Hydrology*, 353: 247–266, 2008.
- B. Andreo, P. Jiménez, J.J. Durán, F. Carrasco, I. Vadillo, and A. Mangin. Climatic and hydrological variations during the last 117-166 years in the south of the Iberian Peninsula, from spectral and correlation analyses and continuous wavelet analyses. *Journal of Hydrology*, 324:24–39, 2006.
- I. Auer, R. Böhm, A. Jurkovic, W. Lipa, A. Orlik, R. Potzmann, W. Schöner, M. Ungersböck, C. Matulla, K. Briffa, P. Jones, D. Efthymiadis, M. Brunetti, T. Nanni, M. Maugeri, L. Mercalli, O. Mestre, J.M. Moisselin, M. Begert, G. Müller-Westermeier, V. Kveton, O. Bochnicek, P. Stastny, M. Lapin, S. Szalai, T. Szentimrey, T. Cegnar, M. Dolinar, M. Gajic-Capka, K. Zaninovic, Z. Majstorovic, and E. Nieplova. HISTALP – historical instrumental climatological surface time series of the Greater Alpine Region. *International Journal of Climatology*, 27:17–46, 2007.
- F. Bataglia and M. Protopapas. Time-varying multi-regime models fitting by genetic algorithms. *Journal of Time Series Analysis*, 32:237–252, 2011.
- J. Beran. *Statistics for long - memory processes*. Chapman and Hall, New York, 1994.
- N. Blasco and R. Santamaría. Testing memory patterns in the Spanish stockmarket. *Applied Financial Economics*, 6:401–411, 1996.
- G. Blöschl and A. Montanari. Climate change impacts - throwing the dice? *Hydrological Processes*, 24:374–381, 2010.
- G. Blöschl, S. Ardoin-Bardin, M. Bonell, M. Dorninger, D. Gutknecht, D. Matamoros, B. Merz, P. Shand, and J. Szolgay. At what scales do climate variability and land cover change impact on flooding and low flows? *Hydrological Processes*, 21:1241–1247, 2007.
- G. E. P. Box and G. M. Jenkins. *Time series analysis forecasting and control*. Holden-Day, San Francisco, 1976.
- P. Brockwell and R. A. Davis. *Introduction to time Series and forecasting*. Springer, 2002.
- P. Burlando, R. Rosso, L.G. Cadavid, and J.D. Salas. Forecasting of short-term rainfall using arma models. *Journal of Hydrology*, 144:193–211, 1993.

- D.H. Burn C.M. Zealand and S.P. Simonovic. Short term streamflow forecasting using artificial neural networks. *Journal of Hydrology*, 214:32–48, 1999.
- N. Crato and B.K. Ray. Model selection and forecasting for long-range dependent processes. *Journal of Forecasting*, 15:107–125, 1998.
- I. Daubechies. *Ten Lectures on Wavelets*. Society for Industrial and Applied Mathematics, Philadelphia, 1992.
- F.X. Diebold and R.S. Mariano. Comparing predictive accuracy. *Journal of Business and Economic Stistics*, 13:253–263, 1995.
- S.L. Dingman. *Physical Hydrology*. Waveland Press, Inc., Long Grove, 2008.
- H. Dou and Y.Q. Chan. Optimal features extraction of noisy sinusoidal signals using two-stage linear least squares fitting. Technical report, Mechatronics and Automation Laboratory, National University of Singapore, 1998. URL <http://www.csois.usu.edu/people/yqchen/>.
- P. Doukhan, G. Oppenheim, and M. S. Taqqu. *Long-range dependence*. Birkhäuser, Boston, 2003.
- E. Ehsanzadeh and K. Adamowski. Autoregressive conditional heteroscedasticity with estimates of the variance of united kingdom inflation. *Econometrica*, 50:987–1008, 1982.
- E. Ehsanzadeh and K. Adamowski. Trends in timing of low stream flows in Canada: Impact of autocorrelation and long - term persistence. *Hydrological Processes*, 24: 970–980, 2010.
- P. Elek and L. Markus. A light - tailed conditionally heteroscedastic model with applications to river flows. *Journal of Time Series Analysis*, 29:14–36, 2007.
- A. Fisher, D. Green, and A. Metcalfe. Modelling of hydrological persistence for hidden state markov decision processes. *Annals of Operations Research*, 199:215–224, 2012.
- A.V. Frolov. Discrete dynamic–stochastic model of long term river runoff variations. *Geophysical Processes*, 38(5):583–592, 2011.
- L. Gaál, J. Szolgay, S. Kohnová, J. Parajka, R. Merz, A. Viglione, and G. Blöschl. Flood timescales: Understanding the interplay of climate and catchment processes through comparative hydrology. *Water Resources Research*, 48:W04511, 2012.
- E. Gelati, H. Madsen, and D. Rosjberg. Markov - switching model for nonstationary runoff conditioned on El Nino information. *Water Resources Research*, 46:W02517, 2010.
- R. Gencay, F. Selcuk, and B. Whitcher. Differentiating intraday seasonalities through wavelet multi - scaling. *Physica A*, 289:543–556, 2001.

- J. Geweke and S. Porter-Hudak. The estimation and application of long memory time series models. *Journal of Time Series Analysis*, 4(4):221–238, 1983.
- P. Grau-Carles. Tests of long memory: a bootstrap approach. *Computational Economics*, 25:103–113, 2005.
- GRDC. *Global Runoff Data Center - Dataset of river discharge time series*. Koblenz, Germany, 2011.
- A. Grinsted, J.C. Moore, and S.Jevrejeva. Application of the cross wavelet transform and wavelet coherence to geophysical time series. *Nonlinear Processes in Geophysics*, 11:561–566, 2004.
- L. Gudmundsson, L.M. Tallaksen, K. Stahl, and A.K. Fleig. Low - frequency variability of European runoff. *Hydrology and Earth System Sciences*, 15:1706–1727, 2011.
- C.J. Harman, P.A. Troch, and M. Sivapalan. Functional model of water balance variability at the catchment scale: 2. Elasticity of fast and slow runoff components to precipitation change in the continental united states. *Water Resources Research*, 48: W02523, 2011.
- D.I. Harvey, S.J. Leybourne, and P. Newbold. Testing the equality of prediction mean squared errors. *International Journal of Forecasting*, 13:281–291, 1997.
- J.W. Hurrell. Decadal trends in the North Atlantic Oscillation: Regional temperatures and precipitation. *Science*, 269:676–679, 1995. doi:10.1126/science.269.5224.676.
- H.E. Hurst. Long-term storage capacity of reservoirs. *Transaction of the American Society of Civil Engineers*, 116:770–779, 1951.
- G. Kaiser. *A friendly Guide to Wavelets*. Birkhäuser, Berlin, 1994.
- M.N Khaliq et al. Identification of hydrological trends in the presence of serial and cross correlations: A review of selected methods and their application to annual flow regimes of Canadian Rivers. *Journal of Hydrology*, 368:117–130, 2009.
- G. Kite. Use of time series analysis to detect climatic change. *Journal of Hydrology*, 111: 259–279, 1989.
- S. K.Jain and K. P. Sudheer. Fitting of hydrologic models: A close look at the nash–sutcliffe index. *Journal of Hydrologic Engineering*, 13:981–986, 2012.
- J. Komorník, M. Komorníková, R.Mesiat, D. Szöeková, and J. Szolgay. Comparison of forecasting performance of nonlinear models of hydrological time series. *Physics and Chemistry on Earth*, pages 1127–1145, 2006.
- M. Komorníková, J. Szolgay, D. Svetlíková, D. Szöeková, and S. Jurčák. A hybrid modelling framework for forecasting monthly reservoir inflows. *Journal of Hydrology and Hydromechanics*, 56(3):145–162, 2008.

- G. Koop, E. Ley, J. Osiewalski, and M.F.J. Steel. Bayesian analysis of longmemory and persistence using arfima models. *Journal of Econometrics*, 76:149–169, 1997.
- E. Koscielny-Bunde, J.W. Kantelhardt, P. Braun, A. Bunde, and S. Havlin. Long - term persistence and multifractality of river runoff records: Detrended fluctuation studies. *Journal of Hydrology*, 322:120–137, 2006.
- D. Koutsoyiannis. Climate change, the Hurst phenomenon, and hydrological statistics. *Hydrological Sciences Journal*, 48:3–24, 2003.
- D. Koutsoyiannis. Hydrological Persistence and the Hurst Phenomenon. In J.H. Lehr and J. Keeley, editors, *The Encyclopedia of Water, Volume 4: Surface and agricultural Water*, page 210–221. Wiley, New York, 2005.
- D. Koutsoyiannis. HESS opinions - a random walk on water. *Hydrology and Earth System Sciences*, 14:585–601, 2010.
- D. Koutsoyiannis and A. Montanari. Statistical analysis of hydroclimatic time series: Uncertainty and insights. *Water Resources Research*, 43, 2007.
- D. Koutsoyiannis, A. Montanari, H.F. Lins, and T.A. Cohn. Discussion of 'The implications of projected climate change for freshwater resources and their management'. *Hydrological Sciences Journal*, 54(2):394–405, 2009.
- W.Z. Kundzewicz, D. Graczyk, T. Maurer, I. Pińskwar, M. Radziejewski, C. Svensson, and M. Szwed. Trend detection in river flow series: 1. Annual maximum flow. *Hydrological Sciences Journal*, 50(5):797–810, 2005.
- H.-H. Kwon, U. Lall, and A. F. Khalil. Stochastic simulation model for nonstationary time series using an autoregressive wavelet decomposition: Applications to rainfall and temperature. *Water. Res. Res.*, 43(5):W05407, 2007. doi:10.1029/2006WR005258.
- D. Labat. Wavelet analysis of the annual discharge records of the world's largest rivers. *Advances in Water Resources*, 31:109–117, 2008.
- M. Lafreniere and M. Sharp. Wavelet analysis of inter-annual variability in the runoff regimes of glacial and nival stream catchments, Bow Lake, Alberta. *Hydrologic Processes*, 17:1093–1118, 2003.
- T. Lee. Serial dependence properties in multivariate streamflow simulation with independent decomposition analysis. *Hydrological Processes*, 26:961–972, 2012.
- H.-L. Liu, A.-M. Bao, X. Chen, L. Wang, and X.-I. Pan. Response analysis of rainfall - runoff processes using wavelet transform: a case study of the alpine meadow belt. *Hydrologic Processes*, 25:2179–2187, 2011.
- A. Lo. Long term memory in stock market prices. *Econometrica*, 59:1279–1313, 1991.
- L.M. Lye and Y.Lin. Long - term dependence in annual peak flows of Canadian rivers. *Journal of Hydrology*, 160:89–103, 1994.

- P. Sibbertsen M. Lohre and T. Könnig. Modeling water flow of the rhine river using seasonal long memory. *Water Resources Research*, 39:W1132, 2003.
- H.R. Maier and G.C. Dandy. Neural networks for the prediction and forecasting of water resources variables: a review of modelling issues and applications. *Environmental Modelling and Software*, 15:101–124, 2000.
- S. Mallat. *A Wavelet Tour of Signal Processing*. Academic Press, New York, 1998.
- M.E. Mann, U. Lall, and B. Salzman. Decadal-to-centennial-scale climate variability: Insights into the rise and fall of the Great Salt Lake. *Nonlinear Proc.Geoph.*, 22(8): 937–940, 1995. doi:10.1029/95GL00704.
- D. Maraun and J. Kurths. Cross wavelet analysis: Significance testing and pitfalls. *Nonlinear Processes in Geophysics*, 11:505–514, 2004.
- D. Markovic and M. Koch. Long-term variations and temporal scaling of hydroclimatic time series with focus on the german part of the elbe river basin. *Hydrological Processes*, 2200:14410–14530, 2013.
- N. Massei, B. Laignel, J. Deloffre, J. Mesquita, A. Motelay, R. Lafite, and A. Durand. Long- term hydrological changes of the seine river flow (france) and their relation to the north atlantic oscillation over the period 1950-2008. *International Journal of Climatology*, 30:2146–2154, 2010.
- A.I. McLeod and K. Hipel. Preservation of the rescaled adjusted range. 1. A reassessment of the Hurst phenomenon. *Water Resources Research*, 14(3):491–508, 1978.
- A.I. McLeod and K. Hipel. *Time Series Modelling of Water Resources and Environmental Systems*. Elsevier, Amsterdam, 1994.
- R. Modarres and T.B.M.J. Ouarda. Generalized autoregressive conditional heteroscedasticity modelling of hydrologic time series. *Hydrological Processes*, 2012.
- R. Modarres and T.B.M.J. Ouarda. Modeling rainfall-runoff relationship using multivariate GARCH model. *Journal of Hydrology*, 2013.
- A. Montanari. Long - range dependence in Hydrology. In P. Doukhan, G. Oppenheim, and M.S. Taqqu, editors, *Theory and applications of long - range dependence*, pages 461–472. Birkhäuser, Boston, 2003.
- A. Montanari, R. Rosso, and M. S. Taqqu. Fractionally differenced ARIMA models applied to hydrologic time series: Identification, estimation, and simulation. *Water Resources Research*, 33:1035–1044, 1997.
- A. Montanari, M. Longoni, and R. Rosso. A seasonal long - memory stochastic model for the simulation of the daily river flows. *Physics and Chemistry of Earth (B)*, 4:319–324, 1999a.

- A. Montanari, M. S. Taqqu, and V. Teverovsky. Estimation of long range dependence in the presence of periodicity: An empirical study. *Mathematical and Computer modelling*, 29:217–228, 1999b.
- A. Montanari, R. Rosso, and M.S. Taqqu. A seasonal fractional ARIMA model applied to the Nile River monthly flows at Aswan. *Water Resources Research*, 36(5):1249–1259, 2000.
- M. Mudelsee. Long memory of rivers from spatial aggregation. *Water Resources Research*, 43(W01202), 2007.
- J. E. Nash and J. V. Sutcliffe. River flow forecasting through conceptual models part i — a discussion of principles? *Journal of Hydrology*, 10:282–290, 1970.
- M. Ooms and P.H. Franses. A seasonal periodic long memory model for monthly river flows. *Environmental Modelling and Software*, 16:559–569, 2001.
- T.J. Osborn, K.R. Briffa, S.F.B. Tett, P.D. Jones, and R.M. Trigo. Evaluation of the North Atlantic Oscillation as simulated by a climate model. *Climate Dyn.*, 15:685–702, 1999. doi:10.1007/s003820050310.
- R. Ouachani, Z. Bargaoui, and T.Ouarda. Power of teleconnection patterns on precipitation and streamflow variability of upper medjerda basin. *International Journal of Climatology*, 33(1):58–76, 2013.
- J. Parajka, S. Kohnová, R. Merz, J. Szolgay, K. Hlavčová, and G. Blöschl. Comparative analysis of the seasonality of hydrological characteristics in Slovakia and Austria. *Hydrological Sciences Journal*, 54(3):456–473, 2009.
- M. Pardé. *Fleuves et rivières 2. ed. rev. et corr.* Colin, Paris, 1947.
- A.I. Pasquini and P.J. Depetris. ENSO - triggered exceptional flooding in the Parana River: Where is the excess water coming from? *Journal of Hydrology*, 383:186–193, 2010.
- M. Patassiová, E. Klementová, T. Litschmann, and M. Čistý. Výskyt sucha a analýza zrážok pri jeho výskyte v jarných mesiacoch (Analysis of the drought and influence of the precipitation on its occurrence during spring months). *Acta Hydrologica Slovaca*, 3:94–101, 2002.
- P. Pekárová, P. Miklánek, and J. Pekár. Spatial and temporal runoff oscillation analysis of the main rivers of the world during the 19th–20th centuries. *Journal of Hydrology*, 274:62–79, 2003.
- P. Pekárová, D. Halmová, V. Bačová Mitková, P. Miklánek, J. Pekár, and J. Škoda. Historic flood marks and flood frequency analysis of the danube river at bratislava. *Journal of Hydrology and Hydromechanics*, 61:326–333, 2013.
- J.D. Pelletier and D.L. Turcotte. Long-range persistence in climatological and hydrological time series: Analysis, modeling and application to drought hazard assessment. *Journal of Hydrology*, 203:198–208, 1997.

- C.K. Peng, S.V. Buldyrev, S. Havlin, M. Simons, H.E. Stanley, and A.L. Goldberger. Mosaic organization of dna nucleotides. *Physical Review E*, 49:1685–1689, 1994.
- C.K. Peng, S. Havlin, H.E. Stanley, and A.L. Goldberger. Quantification of scaling exponents and crossover phenomena in nonstationary heartbeat time series. *Chaos*, 5(1):82–87, 1995.
- T. Petrow, J. Zimmer, and B. Merz. Changes in the flood hazard in Germany through changing frequency and persistence of circulation patterns. *Natural Hazards and Earth Systems Sciences*, 9:1409–1423, 2009.
- C.A. Pires and R.A.P. Perdigao. Non-Gaussianity and Asymmetry of the Winter Monthly Precipitation Estimation from the NAO. *Mon. Wea. Rev.*, 135:430–448, 2007. doi:10.1175/MWR3407.1.
- T.S. Prass, J.M. Bravo, R.T. Clarke, W. Collischonn, and S.R.C. Lopes. Comparison of forecasts of mean monthly water level in the Paraguay River, Brazil, from two fractionally differenced models. *Water Resources Research*, 48:W05502, 2012.
- J. L. Probst and Y. Tardy. Global runoff fluctuations during the last 80years in relation to world temperature change. *American Journal of Science*, 289(3):267 – 285, 1989.
- J.L. Probst and Y. Tardy. Long range streamflow and world continental runoff fluctuations since the beginning of this century. *Journal of Hydrology*, 94:289–311, 1987.
- R.G. Quimpo. Reduction of serially correlated hydrologic data. *Bulletin of the International Association of Scientific Hydrology*, 4:111–118, 1969.
- M. Radziejewski and Z.W. Kundzewicz. Fractal analysis of flow of the river Warta. *Journal of Hydrology*, 200:280–294, 1997.
- W. Rea, L. Oxley, M. Reale, and J. Brown. Estimators for long range dependence: an empirical study. *Electronic Journal of Statistics*, 0:1–16, 2009.
- O. Renaud, J. Starck, and F. Murtagh. Prediction based on multiscale decomposition. In *International Journal of Wavelets Multiresolution and Information Processing*, volume 1, pages 217–232, 2003.
- C. Reszler, G. Blöschl, and J. Komma. Identifying runoff routing parameters for operational flood forecasting in small to medium sized catchments. *Hydrological Sciences Journal*, 53:112–129, 2008.
- N. Rimbu, C. Boronenat, C. Bruta, and M. Dima. Decadal variability of the danube river flow in the lower basin and its relation with the north atlantic oscillation. *Int. J. Climatol.*, 22:1169–1179, 2002. doi:10.1002/joc.788.
- P. M. Robinson. Gaussian semiparametric estimation of time series with long - range dependence. *The Annals of Statistics*, 23:1630–1661, 1995.

- J.C. Rogers. North Atlantic storm track variability and its association to the North Atlantic Oscillation and climate variability of northern Europe. *J. Climate*, 10:1635–1647, 1997.
- O. Rosse. Estimation of the Hurst parameter of long- range dependent time series. Research Report Series 137, University of Würzburg, February 1996.
- J. Song S. Wei and N.I. Khan. Simulating and predicting river discharge time series using a wavelet-neural network hybrid modelling approach. *Hydrological Processes*, 26(2): 281–296, 2012.
- G. Sakalauskiene. The Hurst phenomenon in hydrology. *Environmental Research, Engineering and Management*, 3:16–20, 2003.
- J.D. Salas, D.C. Boes, G.G.S. Pegram, and V.Yevjevich. The Hurst phenomenon as a preasymptotic behavior. *Journal of Hydrology*, 4:1–15, 1979.
- Y.F. Sang. A review on the applications of wavelet transform in hydrology time series analysis. *Athmospheric Research*, 122:8–15, 2013.
- P. Schmocker-Fackel and F. Naef. Changes in flood frequencies in Switzerland since 1500. *Hydrology and Earth System Sciences*, 14:1581–1594, 2010.
- M.J. Shensa. Discrete wavelet transforms: Wedding the à trous and mallat algorithms. In *IEEE Transactions on Signal Processing*, volume 40, pages 2464–2482, 1992.
- J.O. Skoien, G. Blöschl, and A.W. Western. Characteristic space scales and timescales in hydrology. *Water Resources Research*, 39(10):W01304, 2003.
- K. Stahl, H. Hisdal, J. Hannaford, L.M. Tallaksen, H.A.J. van Lanen, E. Sauquet, S. Demuth, M. Fendekova, and J. Jódar. Streamflow trends in Europe: Evidence from a dataset of near - natural catchments. *Hydrology and Earth System Sciences*, 14: 2367–2382, 2010.
- J.L. Starck, F. Murtagh, and A. Bijaoui. *Image processing and data analysis: The multiscale approach*. Cambridge University Press, Cambridge, 1998.
- C. Svensson, W.Z. Kundzewicz, and T. Maurer. Trend detection in river flow series: 2. Flood and low-flow index series. *Hydrological Sciences Journal*, 50(5):811–824, 2005.
- E. Szolgayova, G. Laaha, C. Bucher, and G. Blöschl. Factors influencing long range dependence in streamflow of European rivers. *Hydrological Processes*, 28(4):1573–1586, 2013.
- A.M.G. Klein Tank, J.B.Wijngaard, G.P. Können, R. Böhm, G. Demaré, A. Gocheva, M. Mileta, S. Pashiardis, L. Hejkrlik, C. Kern Hansen, R. Heino, P. Bessemoulin, G. Müller Westermeier, M. Tzanakou, S. Szalai, T. Pálsdóttir, D. Fithzgerald, S. Rubin, M. Capaldo, M. Maugeri, A. Leitass, A. Bukantis, R. Aberfeld, A.F.V. van Engelen, E. Forland, M. Mielus, F. Coehlo, C. Mares, V. Razuzaev, E. Nieplova, T. Cegnar, J. Antonio López, B. Dahlström, A. Moberg, W. Kirchhofer, A. Ceylan, O. Pachuliuk,

- L.V. Alexander, and P. Petrovic. Daily dataset of 20th-century surface air temperature and precipitation series for the European Climate Assessment. *International Journal of Climatology*, 22:1441–1453, 2003. URL <http://www.ecad.eu>.
- M. S. Taqqu and V. Teverovsky. On estimating the intensity of long-range dependence in finite and infinite variance time series. *R.J.Adler, editors: A practical guide to heavy tails*, Birkhäuser, Boston, pages 177–217, 1998.
- V. Teverovsky, M. S. Taqqu, and W. Willinger. Estimator for long-range dependence: An empirical study. *Fractals*, 3(4):785–798, 1995.
- H. Theil. *Economic Forecasting and Policy*. North Holland, Amsterdam, 1958.
- M. Thuillard. A review of wavelet networks, wavenets, fuzzy wavenets and their applications. *Advances in Computational Intelligence and Learning*, 18:43–60, 2002.
- A. Timuhins, V. Rodinovs, and M. Klavins. Wavelet analysis of the baltic region river runoff long - term trends and fluctuations. *Proceedings of the Latvian Academy of Sciences*, 64(5/6):229–235, 2010.
- C. Torrence and G. Compo. A practical guide to wavelet analysis. *Bulletin of the American Meteorological Society*, 79:61–78, 1999.
- C. Torrence and P.J. Webster. Interdecadal changes in the ENSO - Monsoon System. *Journal of Climate*, 12:2679–2690, 1999.
- H. Tyrallis and D. Koutsoyiannis. Simultaneous estimation of the parameters of the Hurst - Kolmogorov stochastic process. *Stochastic Environmental Research and Risk Assessment*, 25:21–33, 2011.
- P. Valent, N. Howden, J. Szolgay, and M. Komorníková. Analysis of nitrate concentrations using nonlinear time series models. *Journal of Hydrology and Hydromechanics*, 59(3): 157–170, 2011.
- B. Vidakovic. *Statistical modelling by wavelets*. John Wiley and Sons, New York, 1999.
- J.V. Vogt, P. Soille, A. de Jager, E. Rimaviciute, W. Mehl, S. Foisneau, K. Bódis, J. Dusart, M.L. Paracchini, P. Haastrup, and C. Bamps. A pan-European River and Catchment Database. Report EUR 22920 EN, EC-JRC, Luxembourg, 2007. URL <http://ccm.jrc.ec.europa.eu/php/index.php?action=view&id=23>. Web accessed November 2011.
- H. Wittenberg. Baseflow recession and recharge as nonlinear storage processes. *Hydrol. Process.*, 13:715–726, 1999. doi:10.1002/(SICI)1099-1085(19990415)13:5<715::AID-HYP775>3.0.CO;2-N.
- S. Yousefi, I. Weinreich, and D. Reinartz. Wavelet-based prediction of oil prices. *Chaos, Solitons and Fractals*, 25:265–275, 2005.

- F. Yusof, I.L. Kane, and Z. Yusop. Structural break or long memory: an empirical survey on daily rainfall data sets across malaysia. *Hydrology and Earth System Sciences*, 17: 1311–1318, 2013.
- Q. Zhang, C.-Y. Xu, Y.D. Chen, and Z.Yu. Multifractal detrended fluctuation analysis of streamflow series of the Yangtze River basin, China. *Hydrological Processes*, 22: 4997–5003, 2008.

Appendix A

Data and estimation results overview from Chapter 2.

Table A-1: Description of the runoff data used in this study, including the Hurst coefficient estimates from all five methods. N_i is the time series length (years), A_i is the catchment area (km^2) and P_i is the mean annual precipitation (mm).

River	Station	Country	N_i	A_i	P_i	Hurst coefficient				
						R/S	Period.	Whittle	A.Var.	LSV
Arhus A	Skibby	DK	164	120	646	0.84	0.98	0.75	0.78	1
Birse	Moutier La Charrue	CH	96	183	1213	0.78	0.83	0.9	0.72	0.91
Cabe	Rivas Altas	ESP	63	353	1230	0.8	0.89	0.89	0.75	0.94
Danube	Achleiten	DE	86	76653	961	0.82	0.9	0.86	0.77	0.99
Danube	Bratislava	SK	94	131331	904	0.83	0.93	0.89	0.75	1
Danube	Kienstock	AT	115	95970	992	0.77	0.89	0.86	0.74	0.98
Danube	Orsova	RO	150	576232	807	0.83	0.96	0.96	0.78	1
Danube	Regensburg	DE	86	35399	846	0.82	0.92	0.91	0.79	0.99
Dora Baltea	Tavagnasco	ITA	59	3313	1563	0.82	0.89	0.89	0.81	0.94
Duero	Herrera de Duero	ESP	63	12740	525	0.78	0.96	0.94	0.8	1
Ebro	Zaragoza	ESP	63	40434	679	0.85	0.84	0.85	0.84	0.96
Elbe	Decin	CZ	88	51123	665	0.82	0.9	0.94	0.73	0.99
Elbe	Dresden	DE	157	53096	664	0.79	0.88	0.87	0.74	0.99
Emme	Emmenmatt	CH	98	443	1288	0.77	0.75	0.79	0.7	0.84
Fulda	Guntershausen	DE	89	6366	793	0.78	0.84	0.82	0.73	0.97
Fusta	Fustvatn	NO	100	520	1868	0.71	0.74	0.84	0.64	0.95
Glama	Elverum	NO	127	15426	646	0.69	0.79	0.73	0.6	0.97
Gudena	Aastedbro	DK	100	187	789	0.76	0.85	0.86	0.71	0.97
Iller	Kempton	DE	80	955	1087	0.72	0.76	0.79	0.64	0.88
La Loire	Montjean	FR	128	110000	751	0.77	0.96	0.91	0.76	1
Lapuanjoki	Keppo	FI	81	3949	567	0.77	0.95	0.77	0.71	1
Lindholm A	Elkaer Bro	DK	101	106	649	0.76	0.83	0.76	0.71	0.97
Lygna	Tingvatn	NO	86	266	1699	0.69	0.75	0.71	0.6	0.94
Maalselv	Malangsfoss	NO	101	3239	612	0.71	0.75	0.59	0.58	0.95
Main	Wuerzburg	DE	185	14031	676	0.78	0.84	0.79	0.74	0.96
Neckar	Plochingen	DE	91	3995	860	0.79	0.83	0.9	0.75	0.93
Oder	Bohumin	CZ	92	4665	742	0.74	0.78	0.76	0.67	0.93
Otta	Lalm	NO	87	3982	1006	0.68	0.7	0.82	0.6	0.95
Rhine	Koeln	DE	194	144232	878	0.78	0.93	0.86	0.73	1
Severn	Bewdley	GB	135	4325	916	0.74	0.79	0.68	0.64	0.95
Stura di Lanzo	Lanzo	ITA	68	582	1279	0.74	0.72	0.76	0.73	0.86
Tanaro	Farigliano	ITA	68	1522	871	0.75	0.82	0.79	0.74	0.88
Tanaro	Montecastello	ITA	68	7985	881	0.73	0.78	0.78	0.76	0.88

Continued on next page

River	Station	Country	N_i	A_i	P_i	R/S	Period.	Whittle	A.Var.	LSV
Thames	Kingston	GB	81	9948	685	0.84	0.97	0.91	0.78	1
Uggerby A	Asted Bro	DK	97	151	651	0.75	0.77	0.73	0.7	0.94
Vah	Sala	SK	107	11218	925	0.77	0.82	0.83	0.69	0.94
Vils	Pfronten Ried	DE	98	110	1090	0.7	0.75	0.78	0.64	0.88
Vosso	Bulken	NO	121	1102	2096	0.73	0.77	0.71	0.67	0.94
Weser	Intschede	DE	152	37720	737	0.83	0.91	0.91	0.79	0.96

Appendix B

Chapter 3 is based on the publication "Factors influencing long range dependence in streamflow of European rivers" by Szolgayova, E., Laaha, G., Blöschl, G., and Bucher, C., *Hydrological Processes*, 2014, Volume 28, Issue 4, pages 1573–1586. The contribution of Elena Szolgayova to this paper was

- Choice of estimation methods and calculation of the Hurst coefficient estimators
- Comparison of the Hurst coefficient estimators
- Calculation and comparison of the correlations between the Hurst coefficient estimators and the external factors.

Chapter 4 is based on the publication "Long term variability of the Danube River flow and its relation to precipitation and air temperature" by Szolgayova, E., Parajka, J., Blöschl, G., and Bucher, C., *Journal of Hydrology*, 2014, Volume 519, Part A, Pages 871–880. The contribution of Elena Szolgayova to this paper was

- The wavelet and cross-wavelet analysis, Hurst coefficient estimation
- Applying of the convolution model, interpretation of the convolution results

Chapter 5 is based on the publication "Wavelet based deseasonalization for modelling and forecasting of daily discharge series considering long range dependence" by Szolgayova, E., Arlt, J., Blöschl, G. and Szolgay, J., *Journal of Hydrology and Hydromechanics*, 2014, Volume 62, Issue 1, Pages 24 - 32. The contribution of Elena Szolgayova to this paper was

- Setting up of the models and adapting the wavelet models for deseasonalization purposes
- Modelling and simulations outputs
- Interpretation of the results